공학석사학위 논문

Novel Photoresponsive Soft Materials based on Highly Emissive Cyanostilbene Derivatives: Studies on Photophysical Property, Liquid Crystalline Behavior

고형광성 시아노스틸벤 유도체를 기반으로 하는 새로운 광응답성 연성재료: 광물리적 특성 및 액정 거동에 대한 연구

2013 년 2 월

서울대학교 대학원

재료공학부

박 진 욱

Novel Photoresponsive Soft Materials based on Highly Emissive Cyanostilbene Derivatives: Studies on Photophysical Property, Liquid Crystalline Behavior

고형광성 시아노스틸벤 유도체를 기반으로 하는 새로운 광응답성 연성재료: 광물리적 특성 및 액정 거동에 대한 연구

지도교수 박 수 영

이 논문을 공학석사 학위논문으로 제출함

2013 년 2 월

서울대학교 대학원

재료공학부

박 진 욱

박진욱의 석사학위논문을 인준함

2013 년 2 월

위 원 장 _____ (인)

부위원장 _____ (인)

위 원 _____ (인)

Novel Photoresponsive Soft Materials based on Highly Emissive Cyanostilbene Derivatives: Studies on Photophysical Property, Liquid Crystalline Behavior

A THESIS SUBMITTED IN PARTIAL FULFILLMENT OF
THE REQUESTMENTS FOR THE DEGREE OF MASTER
IN ENGINEERING AT THE GRADUATE SCHOOL OF
SEOUL NATIONAL UNIVERSITY

February 2012

BY

Jinwook Park

Supervisor

Prof. Soo Young Park

Abstract

Novel Photoresponsive Soft Materials based on Highly Emissive Cyanostilbene Derivatives: Studies on Photophysical Property, Liquid Crystalline Behavior

Jinwook Park

Department of Materials Science and Engineering

The Graduate School

Seoul National University

Photo-responsive materials are promising research areas for a wide range of applications such as optical device, and photo-actuator. Especially, azobenzene, and stilbene based soft materials are commonly known for implementing such applications due to their fast and reversible photo-induced isomerization behavior. Despite those remarkable properties, the molecules show low or non-fluorescence behavior in solid state. In order to solve such problem, fluorescent dyes are attached in azobenzene or stilbene unit via covalent, secondary bonding interactions, or host-guest mixed systems. Nevertheless, at the current stage, there are only a few reports to be successfully demonstrated.

To date, we have reported a novel class of α-cyano-substituted stilbenic derivatives exhibiting a unique and peculiar fluorescence behavior, that is, aggregation-induced enhanced emission (AIEE): it is virtually non-fluorescent in the monomer state in solution but becomes

highly fluorescent upon self-assembly into supramolecules. Furthermore, the cyanostilbene unit in typical AIEE molecules has a multiple function of enabling AIEE-type molecule to undergo a trans-cis photoisomerization, as commonly observed in stilbene and azobenzene materials. However, so far, there is no report on fluorescence property in combination with photoisomerization behavior by using such molecules.

Herein, we report on a demonstration of fluorescence patterning technique via photo-induced isomerization behavior in soft state, LC or soft crystal, based on cyanostilbene derivatives for the first time. The molecules consist of rigid cyanostilbene/dicyanodistrylbenzene(DCS) backbone which shows AIEE behaivor and photo-responsive characters with different lengths of flexible alkoxy chains. In this respect, to clearly understand thermotropic LC and optical property in solid state, we study the following issues: i) the role of –CN group, ii) the role of length of alkyl chain, and iii) understanding of the differences in photoisomerization behavior between cyanostilbene and DCS beackbone. The photo-isomerization behavior is monitored by change of UV-vis abosrbance spectra and confirmed the conversition ratio of trans to cis isomer by ^{1}H NMR data. Based on such characters, we demonstrated a fabrication of fluorescence patterning.

Furthermore, we have synthesized a new cyanostilbene based material, GCS, which forms columnar hexagonal LC phase at room temperature. Thin film of GCS was prepared by spin-coated method. Initially, as-prepared film looks like amorphous state with a high transparency. However, a partial crystallization in the film occurs subsequently. During overnight under dark at near RT (25~30 $^{\circ}$C), it was transformed into the perfectly uniform crystalline film that had same crystal arrangement to GCS bulk powder. In crystalline state, GCS exhibits intense blue fluorescence. Interestingly, such crystalline film shows a soft character. To understand such property, we have carried out GI-XRD measurement. In soft state, GCS shows phase transition behavior via photoisomerization process. Thus, we successfully demonstrate highly fluorescent micro patterns via unique property, so-called photo-tirrgered mass migration behavior, with

phase transition by using soft crystalline material. In this work, we propose a new mechanism of 'photo-triggered mass migration' with phase transition, crystal to LC phase, for the first time.

Keywords: liquid crystal, photoinduced isomerization, fluorescence pattern, mass migration, surface relief grating

Studnet Number: 2011-20645

Contents

List of Tables

List of Schemes

List of Figures

Chapter 1. Introduction

1.1. Aggregation induced enhanced-emission (AIEE)

∏-conjugated organic materials that can assemble into nano- and micrometer-sized self-assembled structures have been found useful in various applications such as organic electronics, and optical devices. However, strong fluorescence from such assemblies is rather uncommon.[1-3] For example, the π-conjugated molecules including stilbene based units exhibit the main absorption band formed by the $S_0 \rightarrow S_1$ transition at around 360 nm. As shown in Figure 1.1, the molecular transition dipole moment μ is mainly oriented along the long molecular axis.[4] Therefore, such molecules are prone to H-type aggregation due to side-by-side oriented molecules with small displacement along the long molecular axis as shown in Figure 1.2. Commonly, absorption spectrum of H-type aggregate is hypsochromically (blue) shifted from that of the solution and exhibits low radiative rate constants k_r owing to the dipole-forbidden nature of the emitting state.[5] Even if the molecules may be highly emissive in the isolated solution state, H-type aggregates generally show concentration quenching behavior. However, contrary to such stilbene based molecule, cyanostilbene materials show entirely opposite PL properties due to their unique twist elasticity.[5] For instance, in case of CN-MBE (See Figure 1.3(a) for its chemical structure), biphenyl and cyanostilbene units are twisted beyond 40°. This twisted structure triggers torsion-induced nonradiative deactivation by avoiding the planar conformation in the S_1 state, thereby rendering the solution non-fluorescent property. However, in solid state, strong intermolecular π-π, hydrogen bonding, and dipole-dipole interactions contributed by the cyano groups cause conformational planarization of the twisted biphenyl and cyanostilbene units and formation of J-type aggregation. Therefore, the cyanostilbene molecules show very strong fluorescence emission in solid state, contrary to the solution state, so-called aggregation-induced enhanced emission (AIEE) behavior.

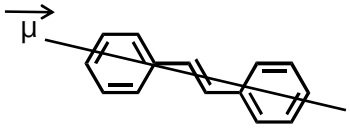

Figure 1.1. Unsubstituted stilbene. The direction of the transition dipole moments are shown as a line.

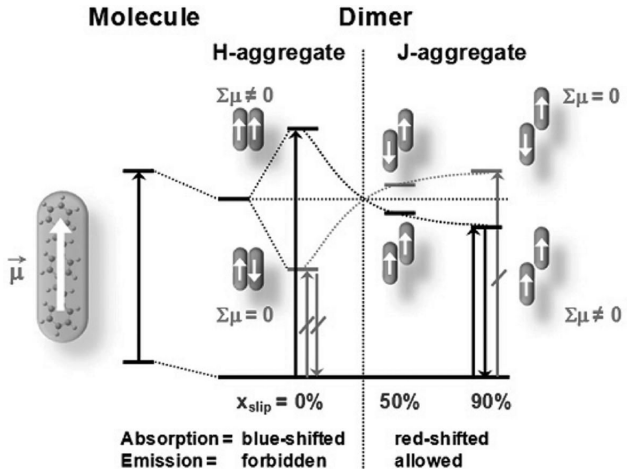

Figure 1.2. H- and J-aggregates and their influence on the absorption and emission processes illlustrated in the framework of exciton models.[5a]

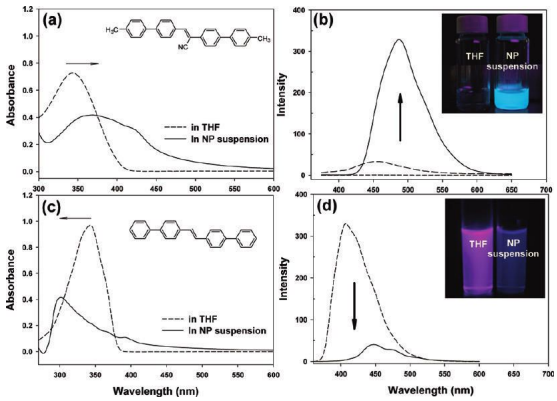

Figure 1.3. UV absorption and PL spectra of CN-MBE (a and b) and DPST (c and d) (2 x 10^{-5} M) in THF and nanoparticle suspensions in 80:20(v/v) water:THF mixture, respectively.[5a]

1.2. Liquid crystal

LCs are 'soft materials' which show mobile and ordered state.[6] For instance, LC can flow like a liquid, while its compounds are more or less oriented in a crystal-like way. LCs can be divided into thermotropic, lyotropic and metallotropic phases. Thermotropic and lyotropic LCs consist of peculiar classes of organic molecules. Thermotropic LCs show temperature dependent a phase transition into the LC phase. Lyotropic LCs exhibit phase transitions as a function of both temperature and concentration of the LC molecules in a solvent (typically water). Metallotropic LCs are composed of both organic and inorganic parts, which means that their LC transition relies not only on the inorganic-organic composition ratio, but also on temperature and concentration. Therefore, a variety of liquid-crystalline (LC) phases have been obtained by tuning the molecular shapes and intermolecular interactions.

Recently, the study of LCs responding to the external stimuli such as light,[7] electric fields,[8] and mechanical shearing,[9] which induce phase transitions, has been actively investigated due to their dynamic and complex properties for potential applications. These LC phase transitions are accompanied by change of the molecular self-assembled structures. Thus, Understanding self-assembled structures is an essential factor to control the properties of LCs.

1.3. Photo-induced isomerization

Stimuli-responsive materials show considerable challenges in the field of material science.[10] The light irradiation among many different external stimuli sources has particular advantages due to very precise, and easily controllable property such as intensity or polarization direction.[11] Naturally occurring photoresponsive systems provide the motivation for developing corresponding artificial systems using molecular self-assembly to address issues such as quantum efficiency, selectivity, and amplification.[10b] General strategy for developing photoresponsive materials is to utilize molecules that can undergo considerable change in shape

upon photoisomerization.[13] Recently, various photo-responsive units are reported such as spiroxy, diarylethene, and butadiene in addition to previously reported azobenzene, and stilbene molecules. Such materials exhibit fast and reversible systems by light and heat stimli. Thus, we could easily control the optical and physical properties with external stimuli.

1.4. Research objectives

Up to now, most of researches have utilized azobenzene, stilbene, and diarylethene materials as photo-responsive units. However, such materials show low or non-fluorecent behavior in solid state even if they exhibit very strong emission in isolated solution state. Contrary to these molecular systems, cyanostilbene unit has very unique performance such as highly enhanced strong emission in solid state, and photoinduced isomerization behavior. However, so far, there has been no report on fluorescence property with photoisomerization behavior by using such molecule.

Herein, we report on the material design, and synthesis of novel AIEE molecules with LC and photoisomerization behavior. We demonstrate highly fluorescent pattern formation from those molecules, which is based on the photoinduced isomerization. Firstly, we designed materials comprising cyanostilbene and dicyanodistrylbenzene (DCS) unit as mesogens core with various length of alkyl chain. We investigated the effects of the length of alkyl chain and backbone structure to the LC performance. Furthermore, the change of fluorescence color was explored as the function of length of alkyl chain and backbone. Lastly, phase transition in LCs triggered by photo isomerization was observed and interpreted. Based on this study, a new concept of fluorescence patterning technique is suggested.

Furthermore, we have synthesized a new cyanostilbene based material, GCS, which forms columnar hexagonal LC phase at room temperature. Thin film of GCS prepared by spin-coating method could be crystallinized into uniform crystalline state. In crystalline state, GCS exhibits

intense blue fluorescence (λ^{max} = 467 nm, Φ_F = 0.22). Interestingly, such crystalline state shows rather 'soft' character. To understand such property, we have carried out GI-XRD measurement. In soft state, GCS shows phase transition behavior via photoisomerization process. Thus, we could successfully demonstrate highly fluorescent micro pattern formation photo-tirrgered mass migration behavior, assisted by the phase transition in the soft crystalline material. In this work, we propose a new mechanism of 'photo-triggered mass migration' which is based on the crystal to LC phase transition for the first time. We believe this work may open up to new possibilities for the optical information application.

The following contents are composed of two different parts:

Chapter 2. Novel Photoresponsive Liquid Crystal System Based on Cyanostilbene Molecules with Aggregation-Induced Enhanced Emission (AIEE): Studies on Mesomorphism, Photochemical Phase Transition Behavior and Photophysical Property.

Chapter 3. Highly Fluorescent Micro patterns via Phototriggered Mass Migration Behavior in Cyanostilbene-based Crystalline Thin Film.

1.5. Bibliography

1. A. Hagfeldt, M. Graetzel, *Chem. Rev.* 1995, *95*, 49.

2. J. Cornil, J. L. Brédas, J. Zaumseil, H. Sirringhaus, *Adv. Mater.* 2007, *19*, 1791.

3. C. Wang, H. Dong, W. Hu, Y. Liu, D. Zhu, *Chem. Rev.* 2011, *112*, 2208.

4. J. Gierschner, M. Ehni, H.-J. Egelhaaf, B. M. Medina, D. Beljonne, H. Benmansour, G. C. Bazan, *J. Chem. Phys.* 2005, *123*, 144914.

5. (a) B.-K. An, J. Gierschner, S. Y. Park, *Acc. Chem. Res.* **2011**, *45*, 544; (b) B.-K. An, S.-K. Kwon, S.-D. Jung, S. Y. Park, *J. Am. Chem. Soc.* **2002**, *124*, 14410. (c) S.-J. Yoon, J. W. Chung, J. Gierschner, K. S. Kim, M.-G. Choi, D. Kim, S. Y. Park, *J. Am. Chem. Soc.* **2010**, *132*, 13675; (d) S.-J. Yoon, J. H. Kim, K. S. Kim, J. W. Chung, B. Heinrich, F. Mathevet, P. Kim, B. Donnio, A.-J. Attias, D. Kim, S. Y. Park, *Adv. Funct. Mater.* **2012**, *22*, 61.

6. (a) J. W. Goodby, D. W. Bruce, M. Hird, C. Imrie, M. Neal, *J. Mater. Chem.* **2001**, *11*, 2631; (b) I. W. Hamley, *Angew. Chem.* **2003**, *115*, 1730; (c) M. D. Hollingsworth, *Science* **2002**, 295, 2410.

7. V. Shibaev, A. Bobrovsky, N. Boiko, *J. Photochem. Photobio. A: Chem.* **2003**, *155*, 3.

8. T. Kato, *Science* **2002**, *295*, 2414.

9. Y. Sagara, T. Kato, *Angew. Chem. Int. Ed.* **2008**, **47**, 5175.

10. (a) J. Zhang, J. K. Whitesell, M. A. Fox, *Chem. Mater.* **2001**, *13*, 2323; (b) S. Das, S. Varghese, N. S. S. Kumar, *Langmuir* **2009**, *26*, 1598; (c) J.-S. Yang, K.-L. Liau, C.-M. Wang, C.-Y. Hwang, *J. Am. Chem. Soc.* **2004**, *126*, 12325; (d) S. Menon, R. Thekkayil, S. Varghese, S. Das, *J. Polym. Sci., Part A: Polym. Chem.* **2011**, **49**, 5063; (e) T. Ubukata, S. Fujii, Y. Yokoyama, *J.Mater. Chem.* **2009**, 19.

11. (a) Y. Yu, M. Nakano, T. Ikeda, *Nature* **2003**, *425*, 145; (b) H. Y. Jiang, S. Kelch, A. Lendlein, *Adv. Mater.* **2006**, *18*, 1471.

12. H. M. D. Bandara, S. C. Burdette, *Chem. Soc. Rev.* **2012**, **41**, 1809.

Chapter 2. Novel Photoresponsive Liquid Crystal System Based on Cyanostilbene Molecules with Aggregation-Induced Enhanced Emission (AIEE): Studies on Mesomorphism, Photochemical Phase Transition Behavior and Photophysical Property

2.1. Introduction

Photo-responsive materials are promising research areas for a wide range of applications such as optical device, and photo-actuator.[1] Especially, azobenzene, and stilbene soft materials are commonly known for implementing such applications due to their fast and reversible photo-induced isomerization behavior. Despite those remarkable properties, the molecules show low or non-fluorescence behavior in solid state.[2] In order to solve such problems, fluorescent dyes are attached in azobenzene or stilbene unit via covalent, secondary bonding interactions, or host-guest mixed systems.[3] Nevertheless, at the current stage, there are only a few reports with successfully demonstrated photo-induced fluorescence switching.

To date, we have reported a novel class of α-cyano-substituted stilbenic derivatives exhibiting a unique and peculiar fluorescence behavior, that is, aggregation-induced enhanced emission (AIEE): they are virtually non-fluorescent in the monomer state in solution but become highly fluorescent upon self-assembly into supramolecules.[4] Recently, we reported a unique discotic hexagonal columnar LC phase at room temperature (RT). Uniaxially aligned LC microwires were fabricated by using the micromolding in capillaries (MIMIC) method whch showed highly enhanced electrical conductivity.[4d] Furthermore, the cyanostilbene unit in typical AIEE molecules has a multiple function of enabling AIEE-type molecule to undergo a trans-cis photoisomerization, as commonly observed in stilbene and azobenzene materials.[5] However, so

far, there has been no report on fluorescence modulation via photoisomerization behavior by using such molecule.

Herain, we report on a demonstration of fluorescence patterning via photoisomerization in LC state based on cyanostilbene derivatives for the first time. The LC system with the fluctuation of free volume is introduced in this work to implement efficiently photoinduced isomerization behavior. The molecules consist of rigid cyanostilbene/dicyanodistrylbenzene(DCS) backbone which shows AIEE behaivor and photo-responsive characters with different lengths of flexible alkoxy chain. In this respect, to clearly understand the nature of LC phase and optical performance in solid state, we study the following issues: i) the role of –CN group, ii) the role of length of the alkyl chain, and iii) understanding of the differences in photoisomerization behavior between cyanostilbene and DCS beackbone. In this work, we could control LC phase and fluorescence color by adjusting the length of alkyl chain and the source of the backbone unit. Furthermore, dual color emission process was observed by changing molecular stacking mode by annealing process. The photo-isomerization behavior was monitored by the change of UV-vis abosrbance spectra. The conversition ratio of trans to cis isomer was observed ^{1}H NMR data. In addition, we could demonstrate highly fluorescence pattern formation via phase transition with photo-isomerization property. Therefore, we report a new class of LC materials which show very unique property by combining AIEE and photoinduced isomerization behavior.

2.2. Results and discussion

2.2.1. Synthesis

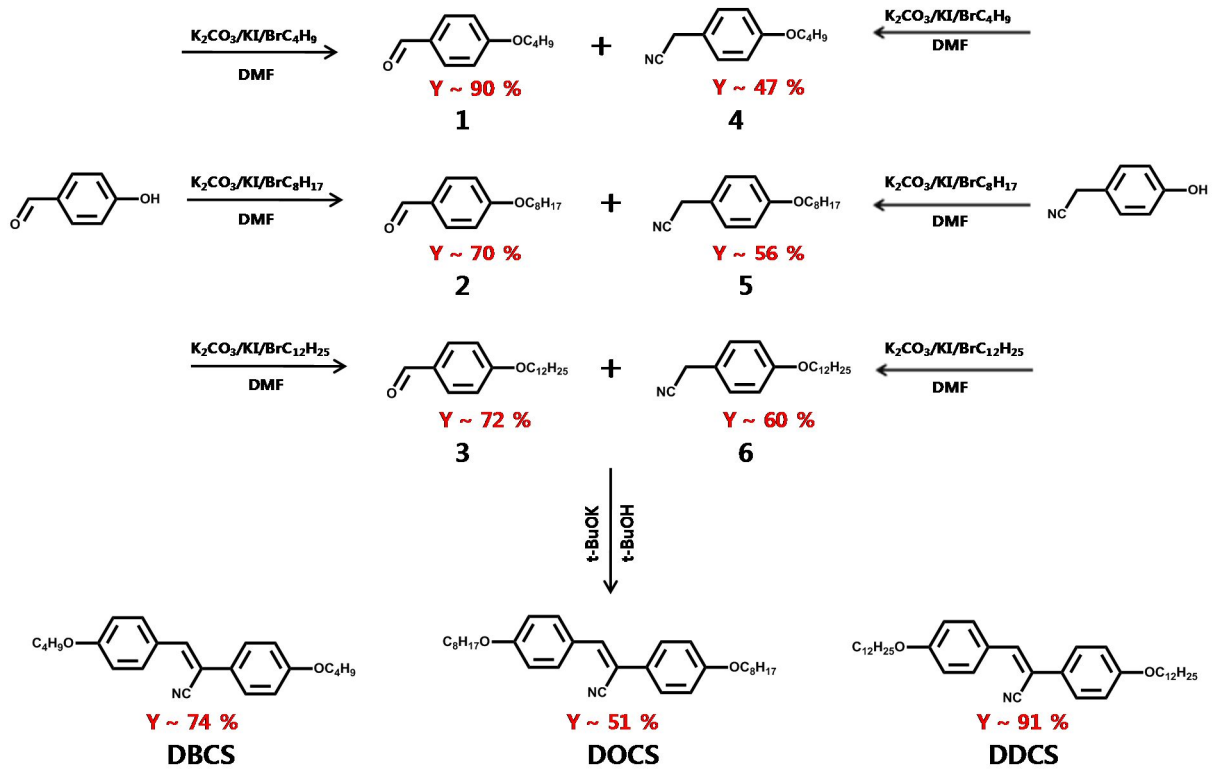

Scheme 2.1. Synthetic scheme of DBCS, DOCS, and DDCS.

4-Butoxy-benzaldehyde (1).

K_2CO_3 (6.79 g, 49.1 mmol) and KI (catalytic amount) were added to a solution of 4-hydroxy-benzaldehyde (5.00 g, 40.9 mmol) in dry DMF (10 mL), and the mixture was stirred at 80 °C. 1-Bromo-butane (5.29 mL, 49.1 mmol) was slowly dropped into the mixture. The reaction lasted overnight. After cooling to room temperature, the mixture was poured into brine and extracted with dichloromethane. The organic phase was dried over $MgSO_4$ and the solvent was evaporated in vacuo. The product (6.55 g, 90 %) was obtained by column chromatography using ethyl acetate and n-hexane (1:10 v/v). 1H NMR (CDCl3) δ [ppm]: 9.88 (s, 1H, -CHO), 7.83 (d,

2H, Ar-H), 6.99 (d, 2H, Ar-H), 4.05 (t, 2H, -OCH_2), 1.80 (m, 2H, -CH_2), 1.51 (m, 2H, -CH_2), 0.99 (t, 3H, -CH_3).

4-Octyloxy-benzaldehyde (2).

K_2CO_3 (6.79, 49.1 mmol) and KI (catalytic amount) were added to a solution of 4-hydroxy-benzaldehyde (5.00 g, 40.9 mmol) in dry DMF (10 mL), and the mixture was stirred at 80 °C. 1-Bromo-octane (7.45 mL, 49.1 mmol) was slowly dropped into the mixture. The reaction lasted overnight. After cooling to room temperature, the mixture was poured into brine and extracted with dichloromethane. The organic phase was dried over $MgSO_4$ and the solvent was evaporated in vacuo. The product (6.71 g, 70 %) was obtained by column chromatography using ethyl acetate and n-hexane (1:10 v/v). 1H NMR (CDCl3) δ [ppm]: 9.88 (s, 1H, -CHO), 7.83 (d, 2H, Ar-H), 6.99 (d, 2H, Ar-H), 4.05 (t, 2H, -OCH_2), 1.80 (m, 2H, -CH_2), 1.51 (m, 10H, -CH_2), 0.99 (t, 3H, -CH_3).

4-Dodecyloxy-benzaldehyde (3).

K_2CO_3 (6.79 g, 49.1 mmol) and KI (catalytic amount) were added to a solution of 4-hydroxy-benzaldehyde (5.00 g, 40.9 mmol) in dry DMF (10 mL), and the mixture was stirred at 80 °C. 1-Bromo-dodecane (11.8 mL, 49.1 mmol) was slowly dropped into the mixture. The reaction lasted overnight. After cooling to room temperature, the mixture was poured into brine and extracted with dichloromethane. The organic phase was dried over $MgSO_4$ and the solvent was evaporated in vacuo. The product (8.54 g, 72 %) was obtained by column chromatography using ethyl acetate and n-hexane (1:10 v/v). 1H NMR (CDCl3) δ [ppm]: 9.88 (s, 1H, -CHO), 7.83 (d, 2H, Ar-H), 6.99 (d, 2H, Ar-H), 4.05 (t, 2H, -OCH_2), 1.80 (m, 2H, -CH_2), 1.51 (m, 18H, -CH_2), 0.99 (t, 3H, -CH_3).

2-(4-butoxyphenyl)acetonitrile (4).

K_2CO_3 (2.49 g, 18.0 mmol) and KI (catalytic amount) were added to a solution of 2-(4-hydroxyphenyl)acetonitrile (2.00 g, 15.0 mmol) in dry DMF (10 mL), and the mixture was stirred at 80 °C. 1-Bromo-butane (1.94 mL, 18.0 mmol) was slowly dropped into the mixture. The reaction lasted overnight. After cooling to room temperature, the mixture was poured into brine and extracted with dichloromethane. The organic phase was dried over $MgSO_4$ and the solvent was evaporated in vacuo. The product (1.14 g, 47.2 %) was obtained by column chromatography using ethyl acetate and n-hexane (1:10 v/v). 1H NMR (CDCl3) δ [ppm]: 7.20 (d, 2H, Ar-H), 6.87 (d, 2H, Ar-H), 4.05 (t, 2H, $-OCH_2$), 3.68 (S, 2H, -CN), 1.80 (m, 2H, $-CH_2$), 1.51 (m, 2H, $-CH_2$), 0.98 (t, 3H, $-CH_3$).

2-(4-(octyloxy)phenyl)acetonitrile (5).

K_2CO_3 (2.49 g, 18.0 mmol) and KI (catalytic amount) were added to a solution of 2-(4-hydroxyphenyl)acetonitrile (2.00 g, 15.0 mmol) in dry DMF (10 mL), and the mixture was stirred at 80 °C. 1-Bromo-octane (2.90 mL, 18.0 mmol) was slowly dropped into the mixture. The reaction lasted overnight. After cooling to room temperature, the mixture was poured into brine and extracted with dichloromethane. The organic phase was dried over $MgSO_4$ and the solvent was evaporated in vacuo. The product (2.07 g, 56.3 %) was obtained by column chromatography using ethyl acetate and n-hexane (1:10 v/v). 1H NMR (CDCl3) δ [ppm]: 7.20 (d, 2H, Ar-H), 6.87 (d, 2H, Ar-H), 4.05 (t, 2H, $-OCH_2$), 3.68 (S, 2H, -CN), 1.80 (m, 2H, $-CH_2$), 1.51 (m, 10H, $-CH_2$), 0.98 (t, 3H, $-CH_3$).

2-(4-(dodecyloxy)phenyl)acetonitrile (6).

K_2CO_3 (2.49 g, 18.0 mmol) and KI (catalytic amount) were added to a solution of 2-(4-hydroxyphenyl)acetonitrile (2.00 g, 15.0 mmol) in dry DMF (10 mL), and the mixture was stirred at 80 °C. 1-Bromo-dodecane (4.31 mL, 18.0 mmol) was slowly dropped into the mixture. The reaction lasted overnight. After cooling to room temperature, the mixture was poured into

brine and extracted with dichloromethane. The organic phase was dried over $MgSO_4$ and the solvent was evaporated in vacuo. The product (2.71 g, 60.2 %) was obtained by column chromatography using ethyl acetate and n-hexane (1:10 v/v). 1H NMR (CDCl3) δ [ppm]: 7.20 (d, 2H, Ar-H), 6.87 (d, 2H, Ar-H), 4.05 (t, 2H, $-OCH_2$), 3.68 (S, 2H, -CN), 1.80 (m, 2H, $-CH_2$), 1.51 (m, 18H, $-CH_2$), 0.98 (t, 3H, $-CH_3$).

(Z)-2,3-bis(4-butoxyphenyl)acrylonitrile (DBCS)

The mixture of **1** (1 g, 5.61 mmol) and **4** (1.06 g, 5.61 mmol) in tert-butyl alcohol (20 mL) was stirred at 50 °C. Tetrabutylammonium hydroxide (TBAH, 1 M solution in methanol, 0.561 mL) was slowly dropped into the mixture and stirred for 20 minutes. The resulting precipitate was filtered and purified by column chromatography using dichloromethane. DBCS bulk powder (1.45 g, 74 %) was obtained by recrystallization from hot ethanol solutions. 1H NMR (CDCl3) δ [ppm]: 7.82 (d, 2H, Ar-H), 7.55 (s, 2H, Ar-H), 7.34 (s, 1H, Vinyl-H), 6.94 (m, 4H, Ar-H), 4.02 (m, 4H, $-OCH_2$), 1.81 (m, 4H, $-CH_2$), 1.52 (m, 4H, $-CH_2$), 1.00 (t, 6H, $-CH_3$).

(Z)-2,3-bis(4-(octyloxy)phenyl)acrylonitrile (DOCS)

The mixture of **2** (1 g, 4.27 mmol) and **5** (1.05 g, 4.27 mmol) in tert-butyl alcohol (20 mL) was stirred at 50 °C. Tetrabutylammonium hydroxide (TBAH, 1 M solution in methanol, 0.427 mL) was slowly dropped into the mixture and stirred for 20 minutes. The resulting precipitate was filtered and purified by column chromatography using dichloromethane. DBCS bulk powder (1.10 g, 56 %) was obtained by recrystallization from hot ethanol solutions. 1H NMR (CDCl3) δ [ppm]: 7.82 (d, 2H, Ar-H), 7.55 (s, 2H, Ar-H), 7.34 (s, 1H, Vinyl-H), 6.94 (m, 4H, Ar-H), 4.02 (m, 4H, $-OCH_2$), 1.81 (m, 4H, $-CH_2$), 1.52 (m, 20H, $-CH_2$), 1.00 (t, 6H, $-CH_3$).

(Z)-2,3-bis(4-(dodecyloxy)phenyl)acrylonitrile (DDCS)

The mixture of **3** (1 g, 3.44 mmol) and **6** (1.04 g, 3.44 mmol) in tert-butyl alcohol (20 mL) was stirred at 50 °C. Tetrabutylammonium hydroxide (TBAH, 1 M solution in methanol, 0.561 mL) was slowly dropped into the mixture and stirred for 20 minutes. The resulting precipitate was filtered and purified by column chromatography using dichloromethane. DBCS bulk powder (1.18 g, 60 %) was obtained by recrystallization from hot ethanol solutions. 1H NMR (CDCl3) δ [ppm]: 7.82 (d, 2H, Ar-H), 7.55 (s, 2H, Ar-H), 7.34 (s, 1H, Vinyl-H), 6.94 (m, 4H, Ar-H), 4.02 (m, 4H, -OCH_2), 1.81 (m, 4H, -CH_2), 1.52 (m, 36H, -CH_2), 1.00 (t, 6H, -CH_3).

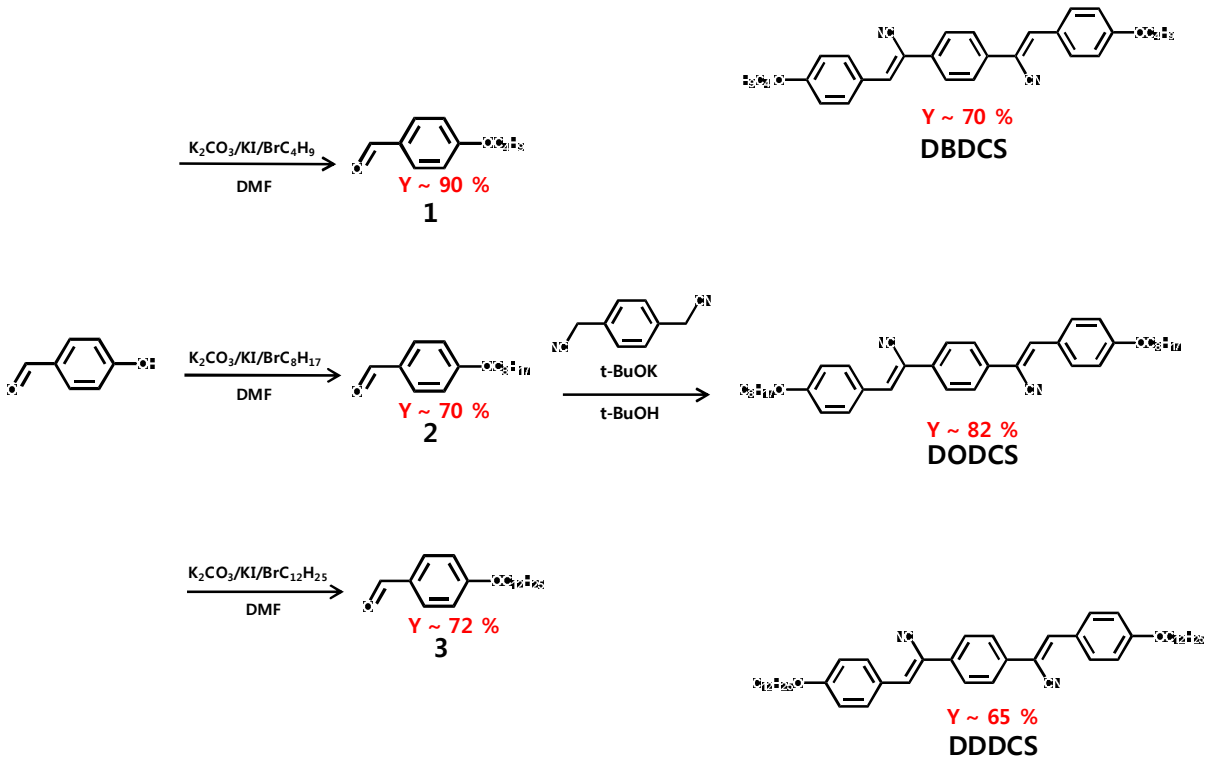

Scheme 2.2. Synthetic scheme of DBDCS, DODCS, and DDDCS.

(2Z,2'Z)-2,2'-(1,4-phenylene)bis(3-(4-butoxyphenyl)acrylonitrile) (DBDCS).

The mixture of 1 (2.00 g, 11.2 mmol) and (4-cyanomethyl-phenyl)-acetonitrile (0.875 g, 5.6

mmol) in tert-butyl alcohol (20 mL) was stirred at 50 °C. Tetrabutylammonium hydroxide (TBAH, 1 M solution in methanol, 1.12 mL) was slowly dropped into the mixture and stirred for 20 minutes. The resulting precipitate was filtered and purified by column chromatography using dichloromethane. DBDCS bulk powder (1.87 g, 70 %) was obtained by recrystallization from hot ethanol solutions. 1H NMR (CDCl3) δ [ppm]: 7.90 (d, 4H, Ar-H), 7.71 (s, 4H, Ar-H), 7.51 (s, 2H, Vinyl-H), 6.98 (d, 4H, Ar-H), 4.04 (t, 4H, $-OCH_2$), 1.81 (m, 4H, $-CH_2$), 1.52 (m, 4H, $-CH_2$), 1.00 (t, 6H, $-CH_3$).

(2Z,2'Z)-2,2'-(1,4-phenylene)bis(3-(4-(octyloxy)phenyl)acrylonitrile) (DODCS).

The mixture of 2 (2.00 g, 8.53 mmol) and (4-cyanomethyl-phenyl)-acetonitrile (0.667 g, 4.27 mmol) in tert-butyl alcohol (20 mL) was stirred at 50 °C. Tetrabutylammonium hydroxide (TBAH, 1 M solution in methanol, 0.853 mL) was slowly dropped into the mixture and stirred for 20 minutes. The resulting precipitate was filtered and purified by column chromatography using dichloromethane. DODCS bulk powder (2.06 g, 82 %) was obtained by recrystallization from hot ethanol solutions. 1H NMR (CDCl3) δ [ppm]: 7.90 (d, 4H, Ar-H), 7.71 (s, 4H, Ar-H), 7.51 (s, 2H, Vinyl-H), 6.98 (d, 4H, Ar-H), 4.04 (t, 4H, $-OCH_2$), 1.81 (m, 4H, $-CH_2$), 1.52 (m, 20H, $-CH_2$), 1.00 (t, 6H, $-CH_3$).

(2Z,2'Z)-2,2'-(1,4-phenylene)bis(3-(4-(dodecyloxy)phenyl)acrylonitrile) (DDDCS).

The mixture of 3 (2.00 g, 6.89 mmol) and (4-cyanomethyl-phenyl)-acetonitrile (0.807 g, 3.44 mmol) in tert-butyl alcohol (20 mL) was stirred at 50 °C. Tetrabutylammonium hydroxide (TBAH, 1 M solution in methanol, 0.689 mL) was slowly dropped into the mixture and stirred for 20 minutes. The resulting precipitate was filtered and purified by column chromatography using dichloromethane. DBDCS bulk powder (1.57 g, 65 %) was obtained by recrystallization from hot ethanol solutions. 1H NMR (CDCl3) δ [ppm]: 7.90 (d, 4H, Ar-H), 7.71 (s, 4H, Ar-H), 7.51 (s, 2H, Vinyl-H), 6.98 (d, 4H, Ar-H), 4.04 (t, 4H, $-OCH_2$), 1.81 (m, 4H, $-CH_2$), 1.52 (m,

36H, -CH_2), 1.00 (t, 6H, -CH_3).

2.2.2. Optical property

We studied the optical property of target materials in solution and nanoparticles. In this work, we could answer a question: the role of –CN group and length of alkyl chain for aggregation behavior with photoluminescence performance. As shown in Figure 2.2, the nanoparticles of cyanostilbene compounds (DBCS, DOCS, DDCS) show bathochromic (red) shift against solution in UV/visible spectra. It means that the aggregation stacking mode is J-type aggregation. However, AIEE behavior is rather weak showing less than ten times enhancement in their fluorescent quantum yields. Nevertheless, the longer length of alkyl chain induced the stronger AIEE behavior (see Figure 2.2 b). In contrast to cyanostilbene backbone system, DCS type system shows very stronger AIEE behavior as shown in Figure 2.3. Furthermore, the nanoparticles exhibit hypsochromic (blue) shift against solution in UV/visible spectra. It means that the stacking mode in solid state is H-type aggregation. Commonly, H-type aggregation induces fluorescence quenching behavior.[2] However, as already reported earlier in our group, AIEE is occurring due to the twist elasticity. It has been also shown that the H-type aggregation is not perfectly H-type and forms excimer aggregation.[4c] As a result, the max value of emission wavelength shows a red shift in photoluminescent spectra. We can deduce that the crystallinity of DCS type is stronger than cyanostilbene type. To clearly understand it, we should study the related photophysics in detail. The photophysical properties of target materials are summarized in Table 2.1.

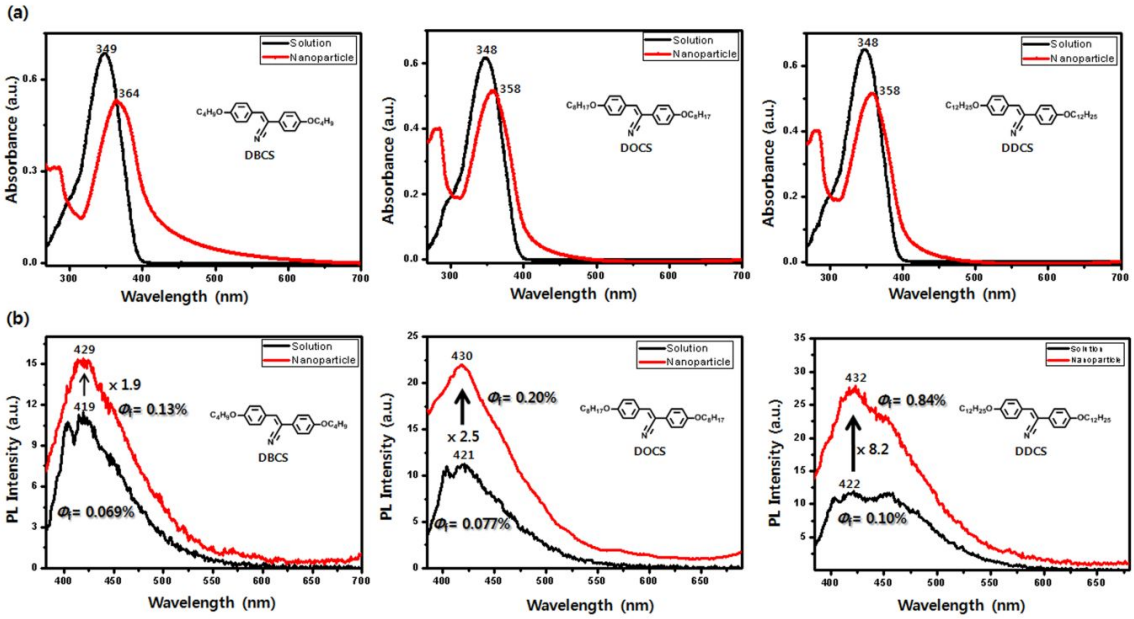

Figure 2.1. UV-visible absorption (a) and photoluminescence (b) spectra of DBCS, DOCS, and DDCS in THF solution (c = 2 x 10^{-5} mol L^{-1}, black line) and a nanoparticles in THF/water mixture (c = 2 x 10^{-5} mol L^{-1}, red line).

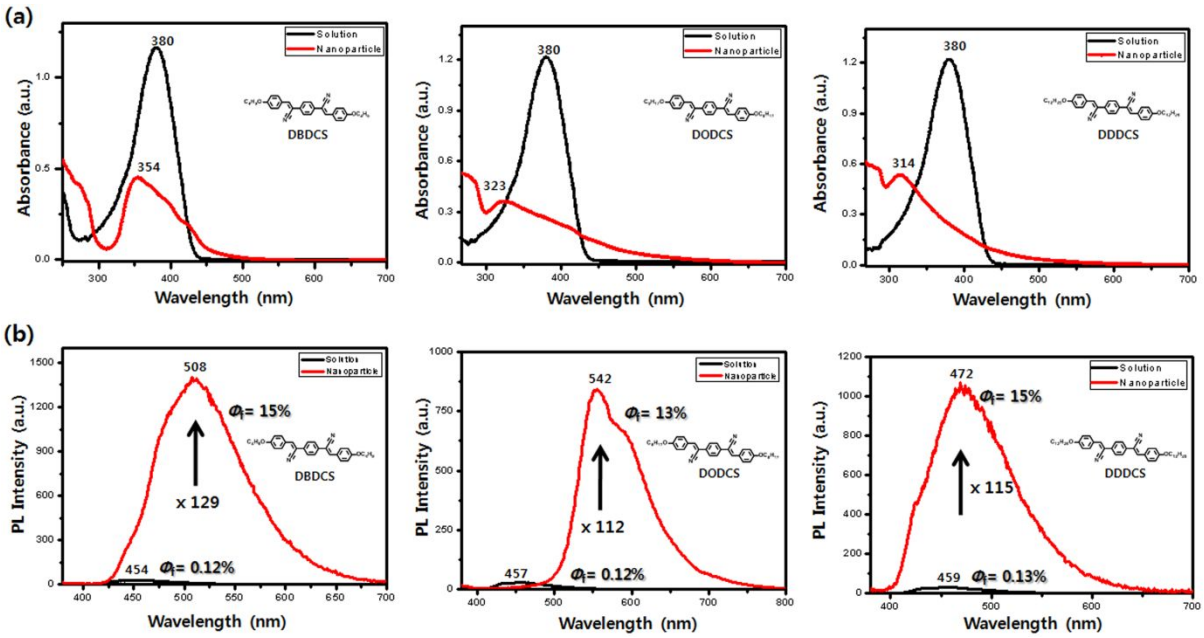

Figure 2.2. UV-visible absorption (a) and photoluminescence (b) spectra of DBDCS, DODCS, and DDDCS in THF solution (c = 2 x 10^{-5} mol L^{-1}, black line) and a nanoparticles in THF/water mixture (c = 2 x 10^{-5} mol L^{-1}, red line).

Table 2.1. Photophysical properties of target materials in THF solution (c = 2 x 10^{-5} mol L^{-1}) and nanoparticles in THF/water mixture (c = 2 x 10^{-5} mol L^{-1}). Excitation wavelength is 360 nm. The relative quantum yield is measured by using 9, 10-diphenylanthracence (DPA) in benzene as a standard reference (1 × 10^{-4} mol L^{-1}, $\Phi_f = 0.83$).

Molecules	λ^{max}_{abs} [nm][a]	λ^{max}_{abs} [nm][b]	λ^{max}_{em} [nm] [a]	λ^{max}_{em} [nm] [b]	Φ_f [%][a]	Φ_f [%][b]
DBCS	349	364	419	429	0.069	0.13
DOCS	348	358	421	430	0.077	0.20
DDCS	348	358	422	432	0.10	0.84
DBDCS	380	354	454	508	0.12	15
DODCS	380	323	457	542	0.16	13
DDDCS	380	314	459	472	0.13	12

[a] Solution state. [b] Nanoparticles state.

2.2.3. Liquid crystal & crystallization property

As shown in Figure 2.4–2.9, all of the target materials show LC phase in both cooling and heating process (the enthalphy value and phase transition temperature are indicated). The mesomorphic properties of target materials were investigated by using polarized optical microscopy (POM) and differential scanning calorimetry (DSC). It was observed that DCS type materials have higher phase transition temperature due to strong secondary bonding intermolecular interactions as we observed in the photophysical property (See above section). The textures of LC phases in target materials suggested nematic, or smectic phases as observed

typically LC: marbled, fan-shaped, sand-like texture. As summarized in Figure 2.10, nematic phase was observed for the butyloxy chains while smectic phase was observed for the longer alkoxy chains. It means that increasing length of alkyl chain induces higher ordered self-assembled LC phase.

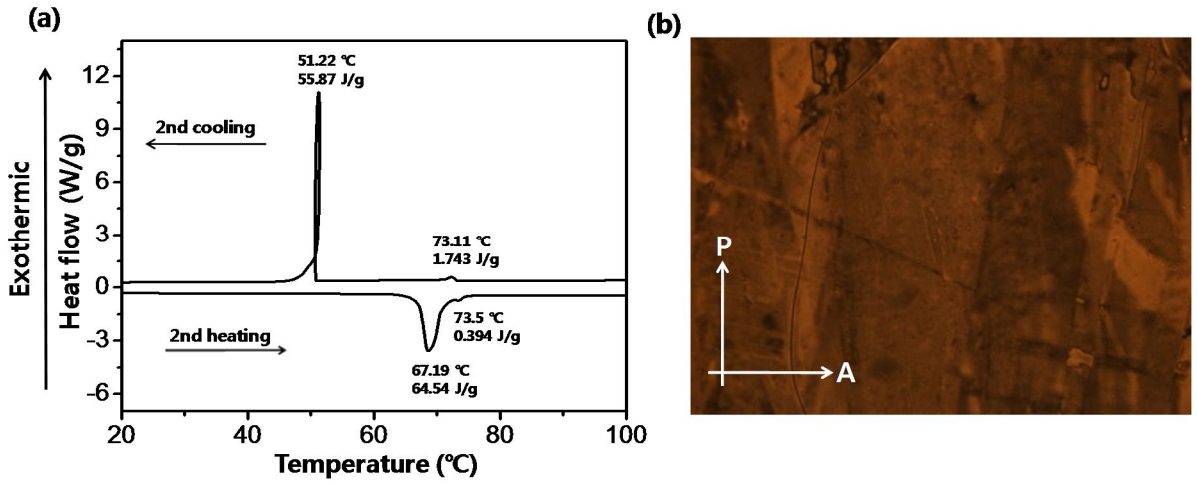

Figure 2.3. (a) DSC trace of DBCS on heating/cooling rate of 10 °C per minute, (b) The nematic liquid crystalline phase was observed by POM at 60 °C on cooling.

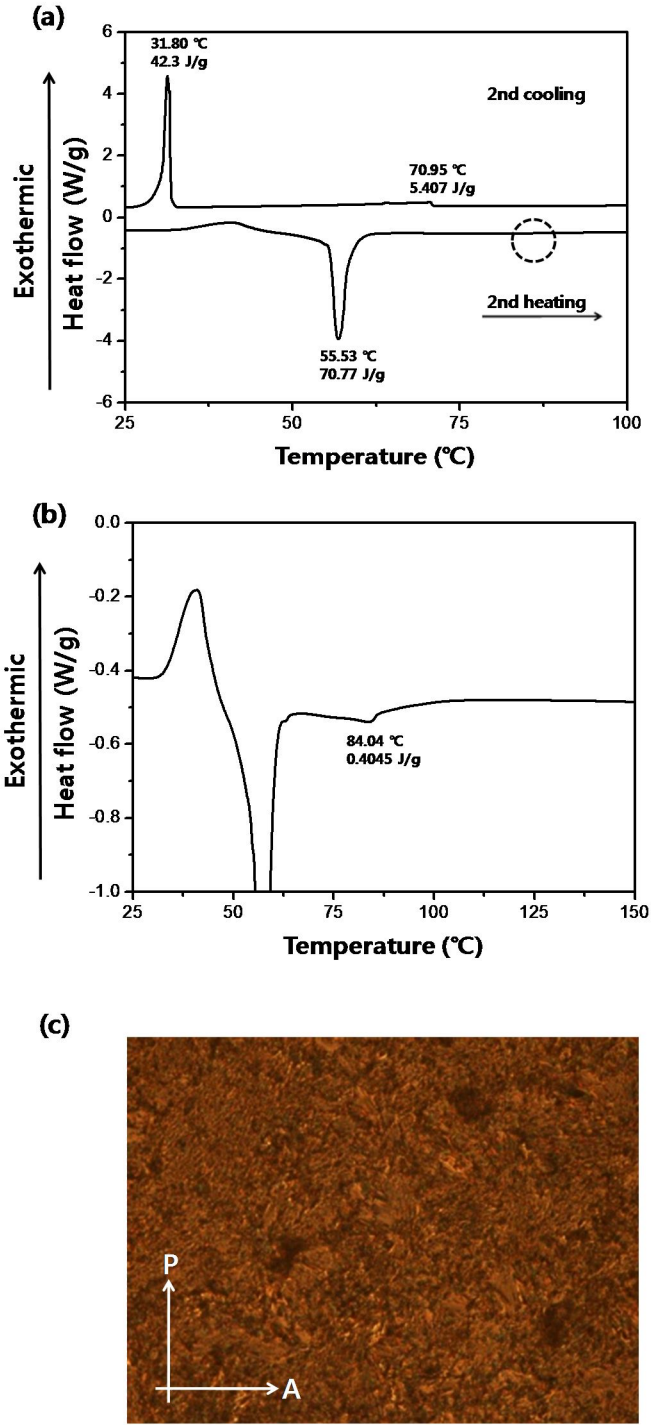

Figure 2.4. (a) DSC trace of DOCS on heating/cooling rate of 10 °C per minute, (b) magnified thermogram of dot circle region. (c) The smectic liquid crystalline phase was observed by POM at 60 °C on cooling.

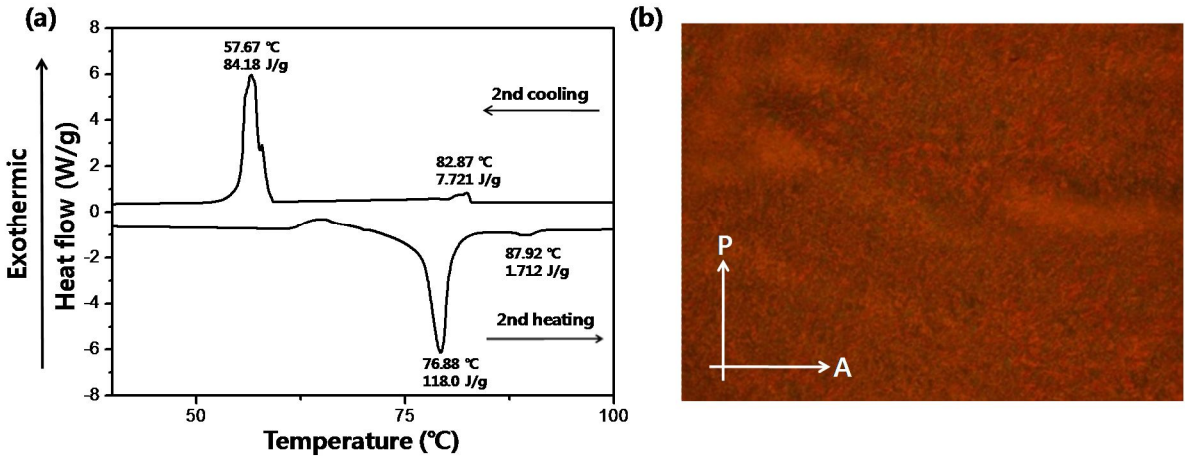

Figure 2.5. (a) DSC trace of DOCS on heating/cooling rate of 10 °C per minute. (b) The smectic liquid crystalline phase was observed by POM at 60 °C on cooling.

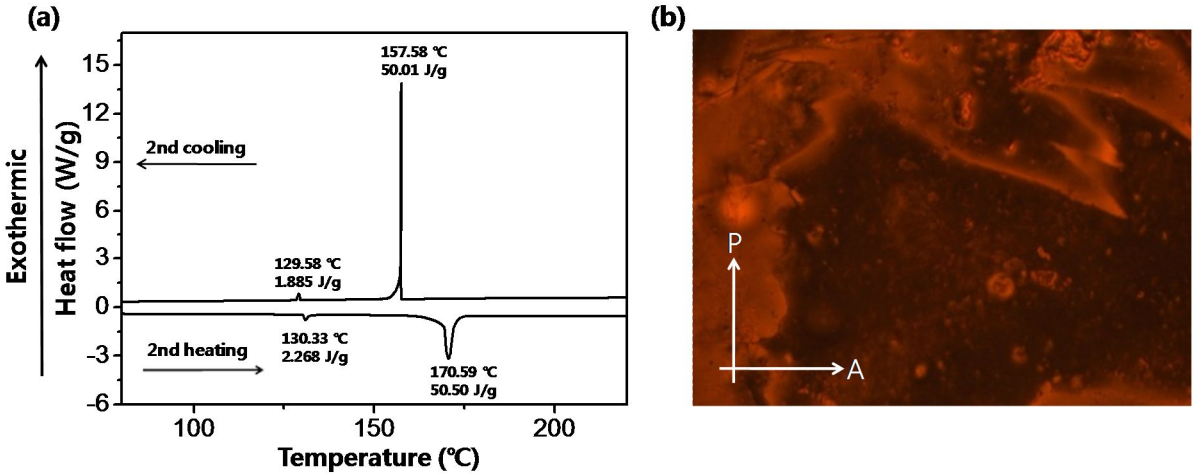

Figure 2.6. (a) DSC trace of DBDCS on heating/cooling rate of 10 °C per minute. (b) The nematic liquid crystalline phase was observed by POM at 140 °C on cooling.

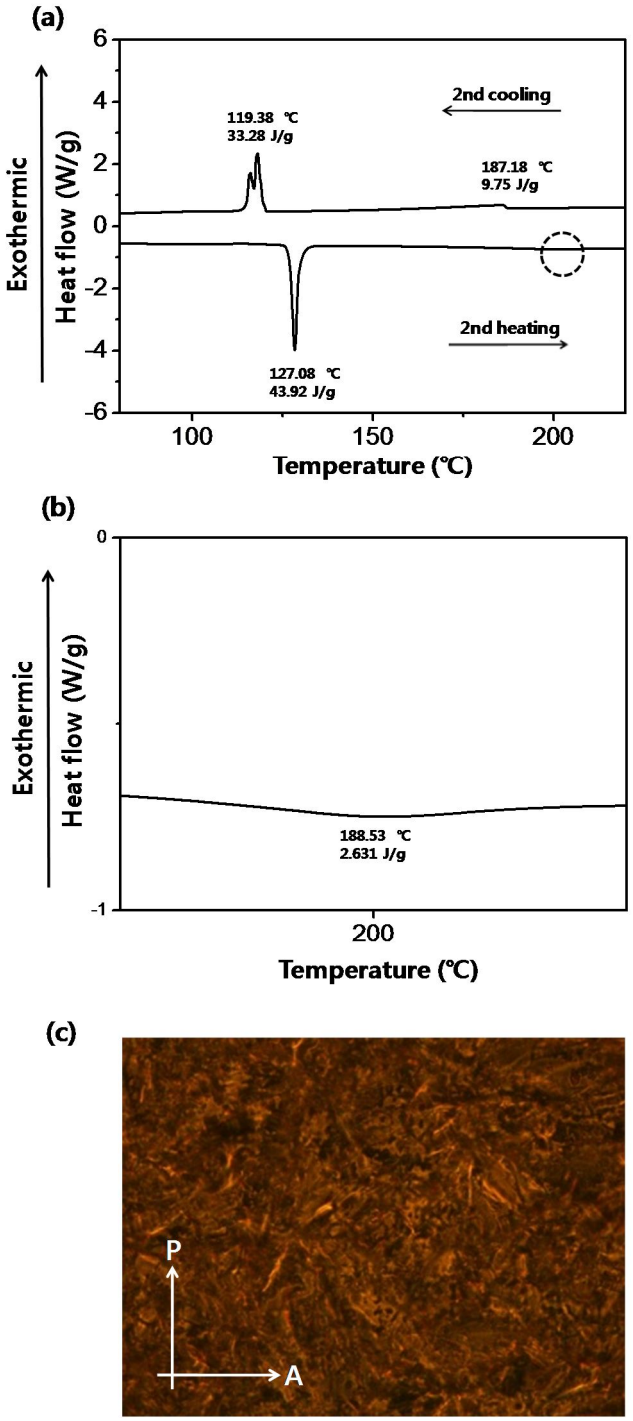

Figure 2.7. (a) DSC trace of DODCS on heating/cooling rate of 10 °C per minute, (b) magnified thermogram of dot circle region. (c) The smectic liquid crystalline phase was observed by POM at 150 °C on cooling.

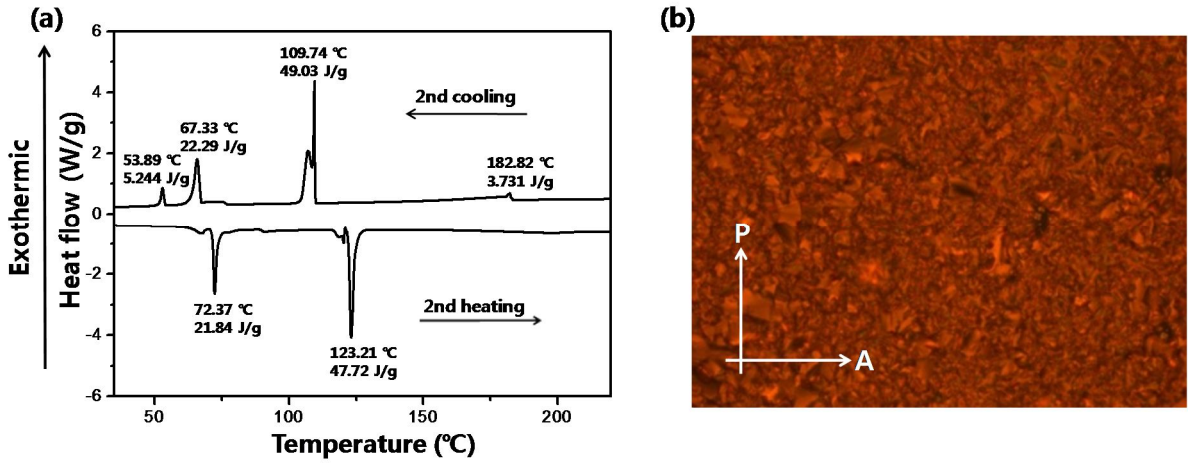

Figure 2.8. (a) DSC trace of DDDCS on heating/cooling rate of 10 °C per minute. (b) The smectic liquid crystalline phase was observed by POM at 150 °C on cooling.

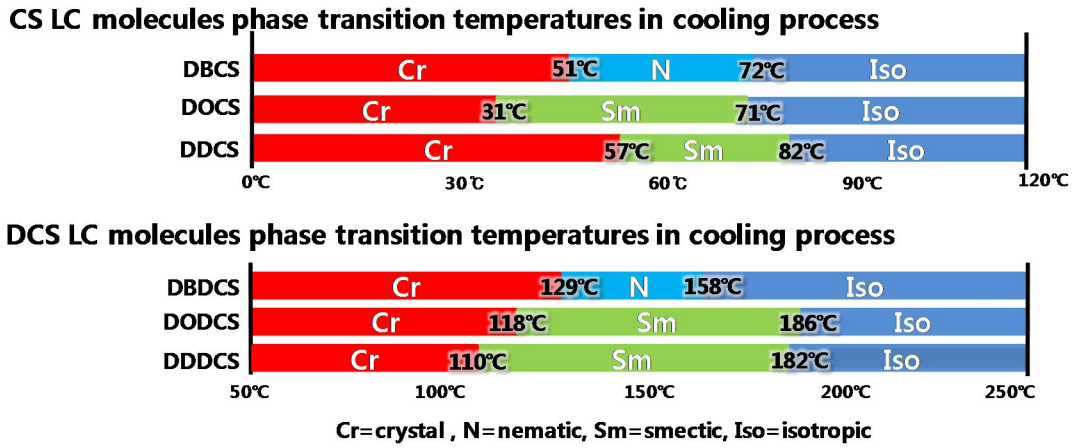

Figure 2.9. Summary of LC phase as a function of temperature: DBCS, DOCS, DDCS, DBDCS, DODCS, and DDDCS.

2.2.4. Photoisomerization

2.2.4.1. Solution state

To study photoinduced isomerization behavior of the target materials, we selected the DBCS molecule for studying photochemistry due to its simplest structure. The cyanostilbene unit exhibits the photoinduced trans-cis isomerization. As shown in Figure 2.11, we observed the evolution of UV-visible absorption spectra of the solution state of DBCS (2×10^{-5} M) according to UV light irradiation, which promoted the trans to cis photoisomerization. Upon irradiation with the 365 nm UV (1 mW cm^{-2}), the absorption band at 348 nm of trans-DBCS decreased and new absorption bands at 244 and 288 nm appeared with one isosbestic point at 321nm. The generated cis isomer exhibited a blue-shift in the absorption wavelength as compared to trans isomer because of the reduced effective conjugation length of the bent conformation. The photo-stationary state (PSS) was reached in about 2 min 30 s in solution. From ^{1}H NMR spectroscopy of Figure 2.12, the resulting conversion ratio of tran to cis is estimated to be 77 % at the photostationary equilibrium state.

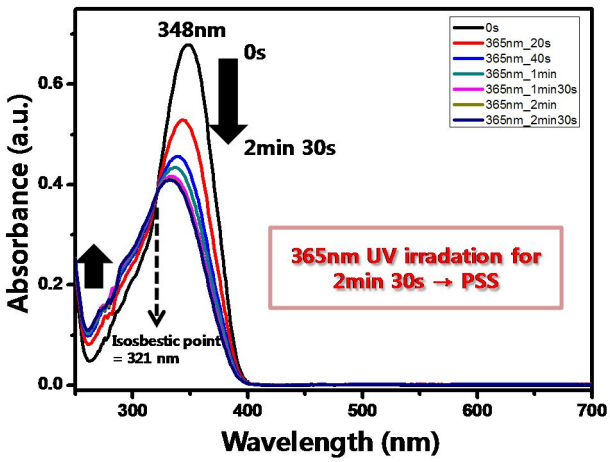

Figure 2.10. Photoisomerization behavior of DBCS in THF solution (2×10^{-5} M): changes in the UV-vis absorption spectra during 365 nm UV light (1 mW cm^{-2}) irradiation at room temperature.

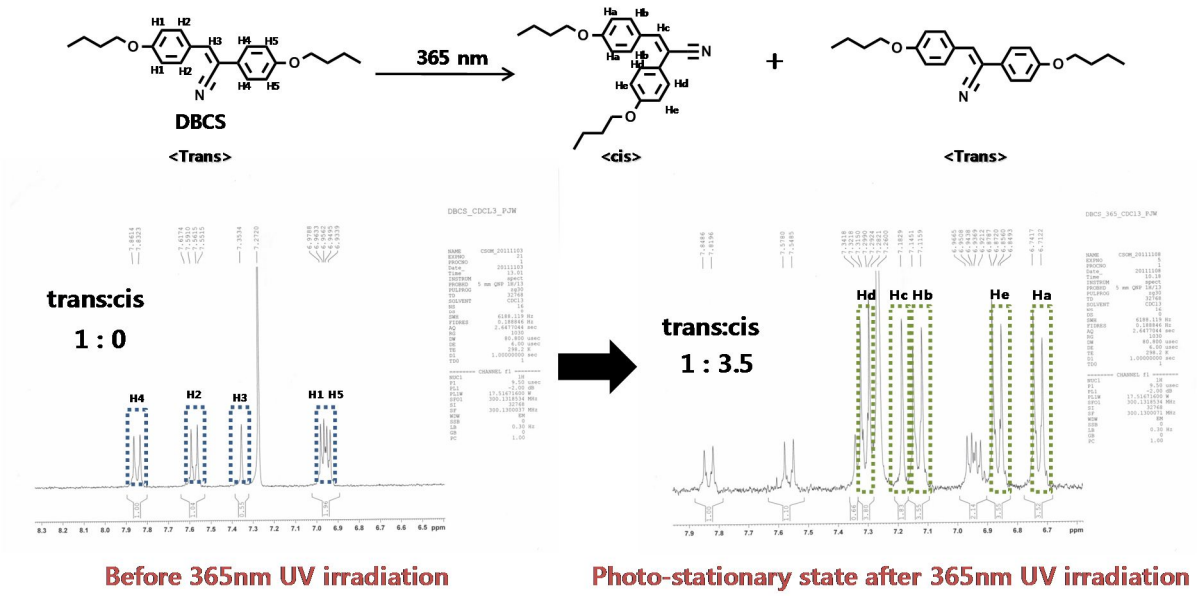

Figure 2.11. ^{1}H NMR spectra (300 MHz, $CDCl_3$, 298 K) of DBCS before UV irradiation (c) after UV irradiation (green dot: cis form).

2.2.4.2. LC state

To control photo-induced isomerization behavior in LC phase, we have monitored the change of LC texture with UV irradiation on LC phase as shown in Figure 2.13–2.18. Regardless of the nature of LC phase, all the moleucles showed phase transition from LC to isotropic phase (See Figure 2.13b–2.18b) upon photoirradiation. However, in cooling process at RT without UV exposure, the crystallization was observed very quickly as shown in Figure 2.13c–2.18c. In crystal state, the strong fluorescence emission was observed (See Figure 2.13d–2.18d). However, fluorescence emission of DBCS crystal is very weak due to relatively weak intermolecular

interactions. The most interesting thing is that the crystalinity and fluorescence property of DDDCS crystal are different from those of other molecules as shown in Figure 2.18c,d. It means that the DDDCS material shows crystal polymorphism upon photoirradiation. Thus, DDDCS molecule could form another crystal phase, unlike other materials. Through this process, we can observe different color or fluorescence qunching behavior in DDDCS crystal via photoinduced isomerization. The only one possibility of fluorescence patterning process in LC phase with phase transition is shown in DDDCS molecule. Next part, we demonstrate a fabrication of clear image of fluorescence pattern by using DDDCS material.

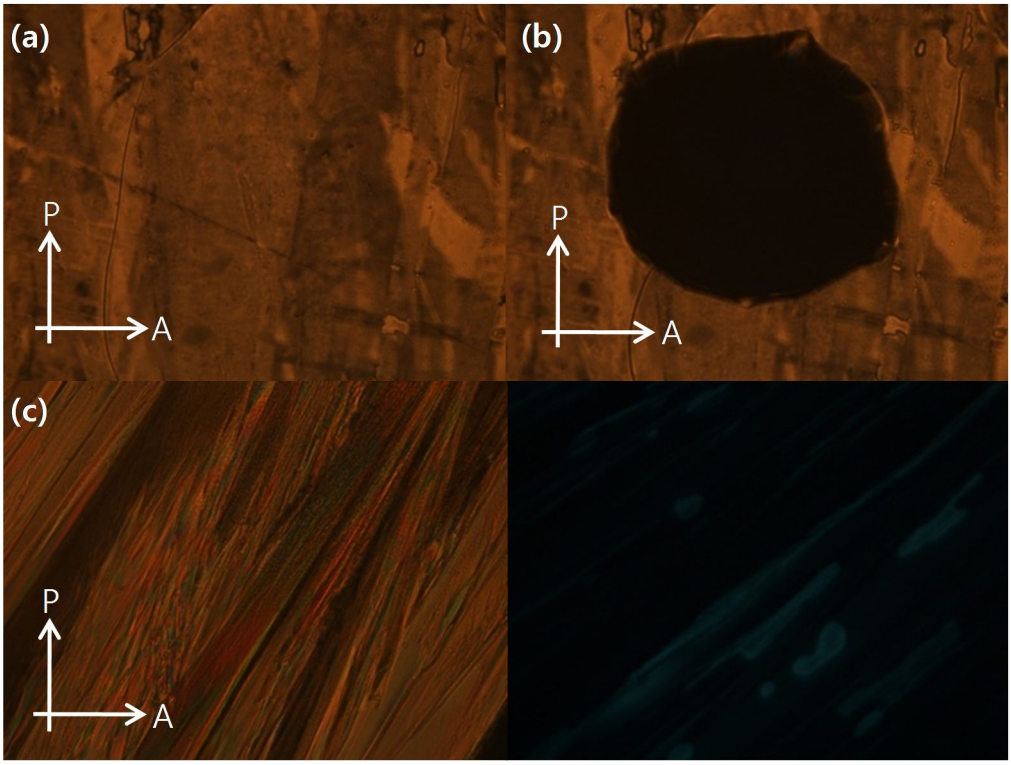

Figure 2.12. (a) The marbled texture image in LC state of DBCS at 50 °C. (b) Phase transition (nematic to isotroipic phase) by UV irradiation, (c) the image of crystal phase in cooling process, and (d) fluorescence image.

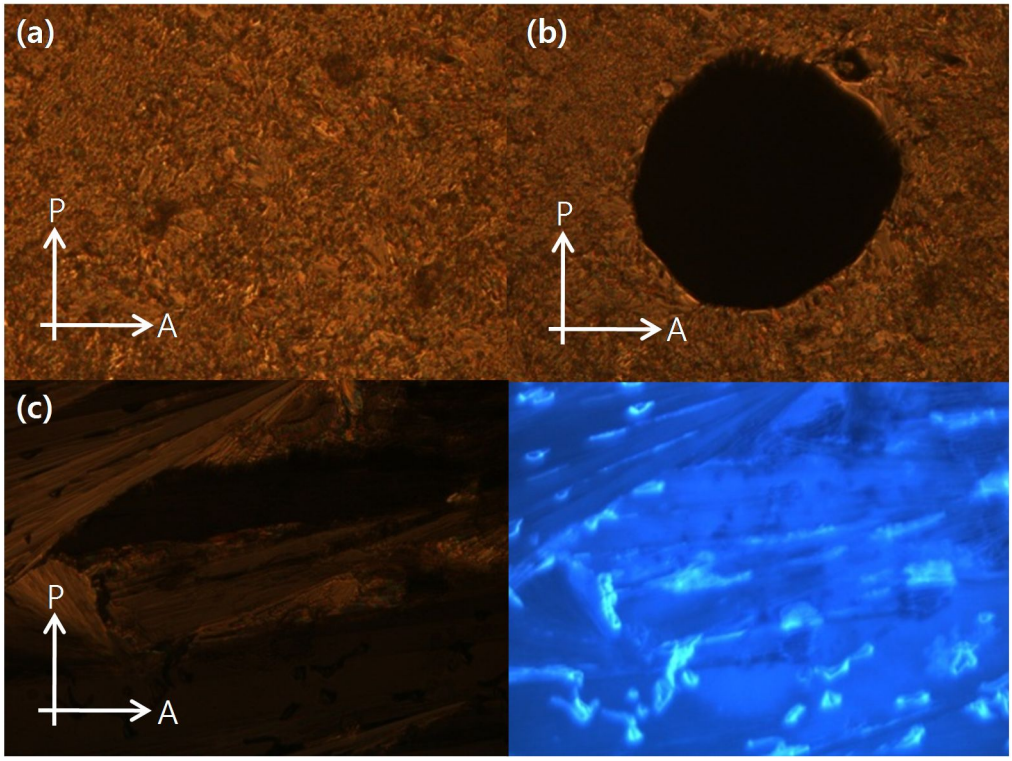

Figure 2.13. (a) The fan-shaped texture image in LC state of DOCS at 50 °C. (b) Phase transition (smectic to isotroipic phase) by UV irradiation, (c) the image of crystal phase in cooling process, and (d) fluorescence image.

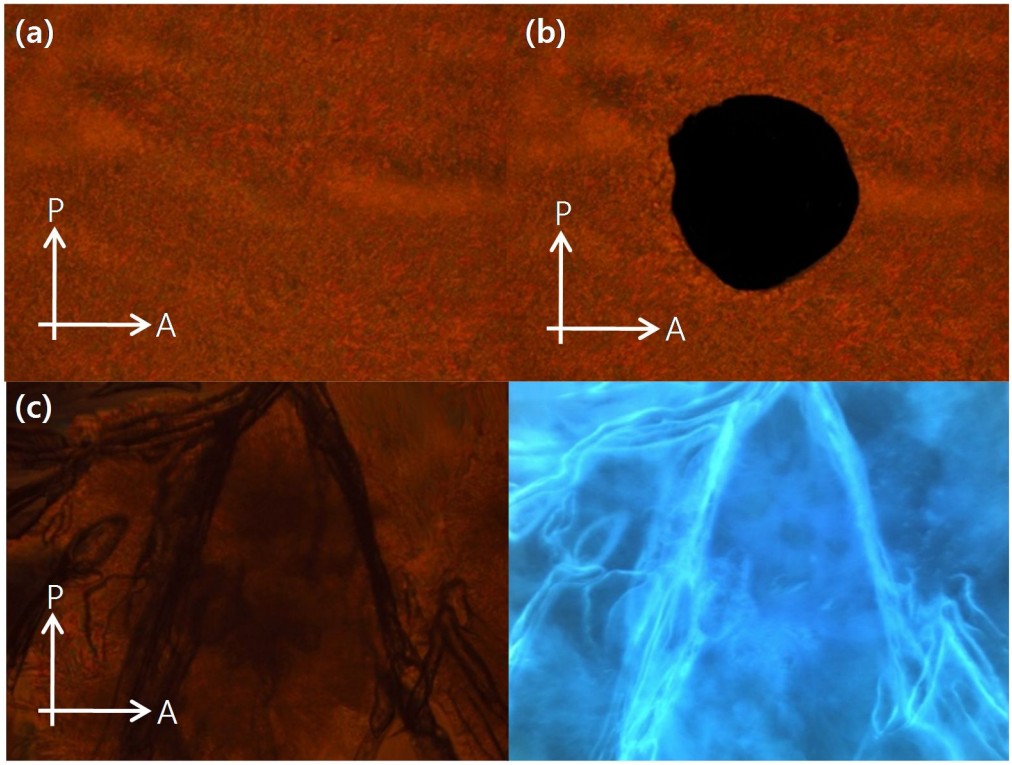

Figure 2.14. (a) The sand-shaped texture image in LC state of DDCS at 50 °C. (b) Phase transition (smectic to isotroipic phase) by UV irradiation, (c) the image of crystal phase in cooling process, and (d) fluorescence image.

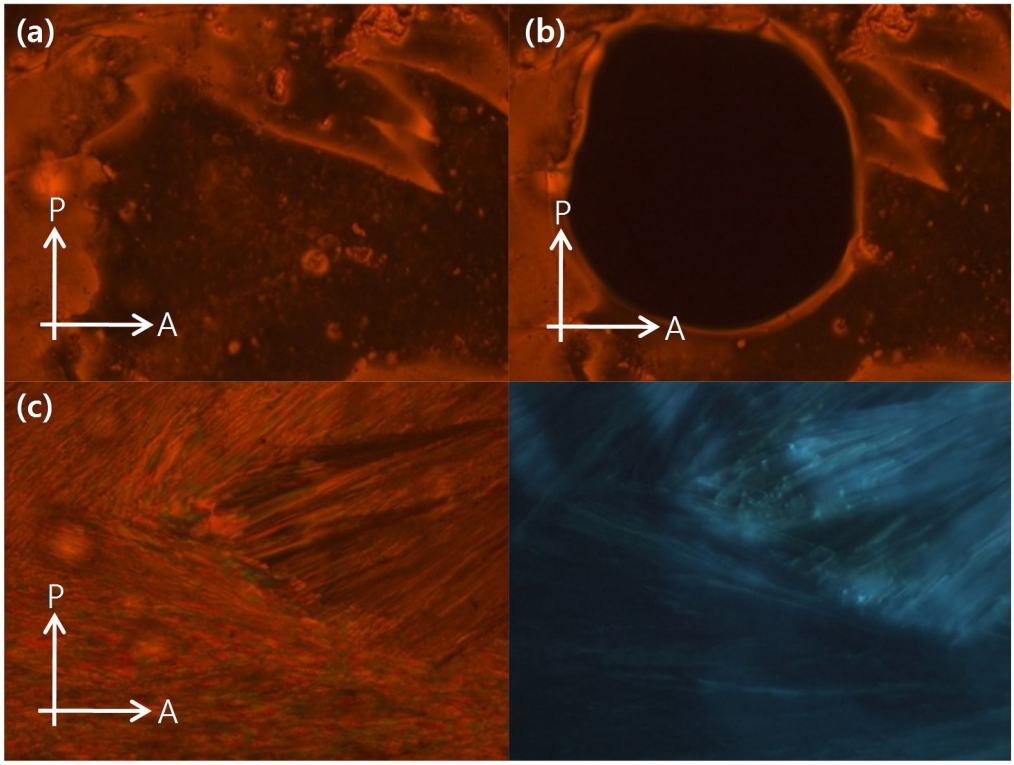

Figure 2.15. (a) The marbled-shaped texture image in LC state of DBDCS at 140 °C. (b) Phase transition (nematic to isotroipic phase) by UV irradiation, (c) the image of crystal phase in cooling process, and (d) fluorescence image.

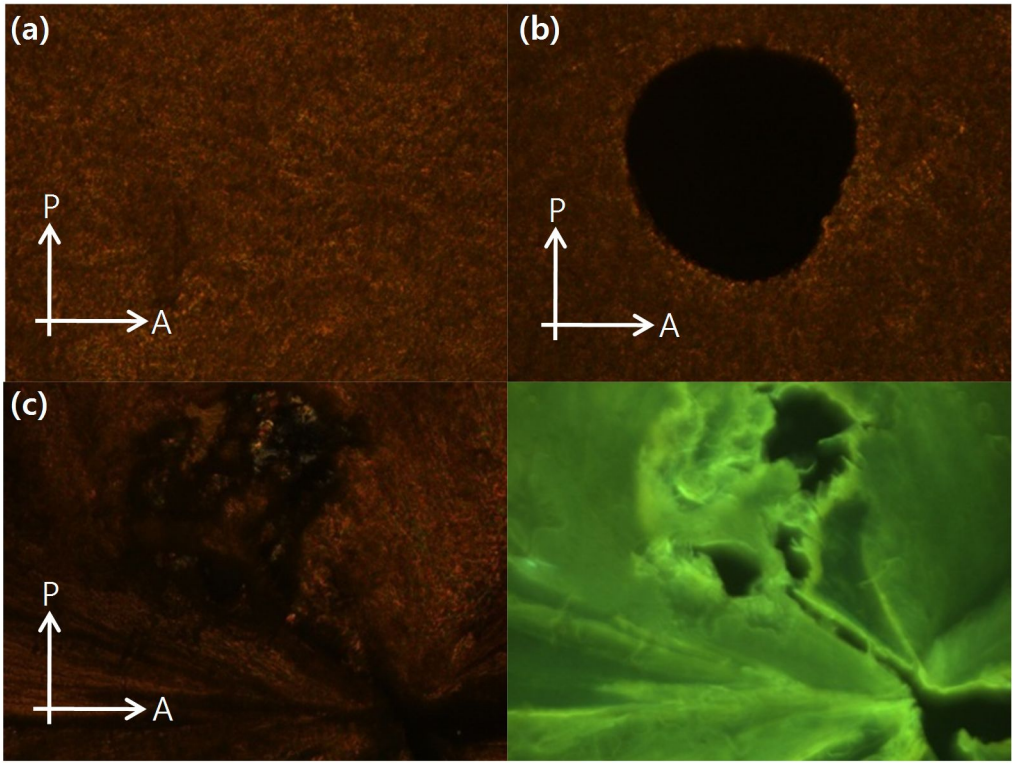

Figure 2.16. (a) The fan-shaped texture image in LC state of DODCS at 150 °C. (b) Phase transition (smectic to isotroipic phase) by UV irradiation, (c) the image of crystal phase in cooling process, and (d) fluorescence image.

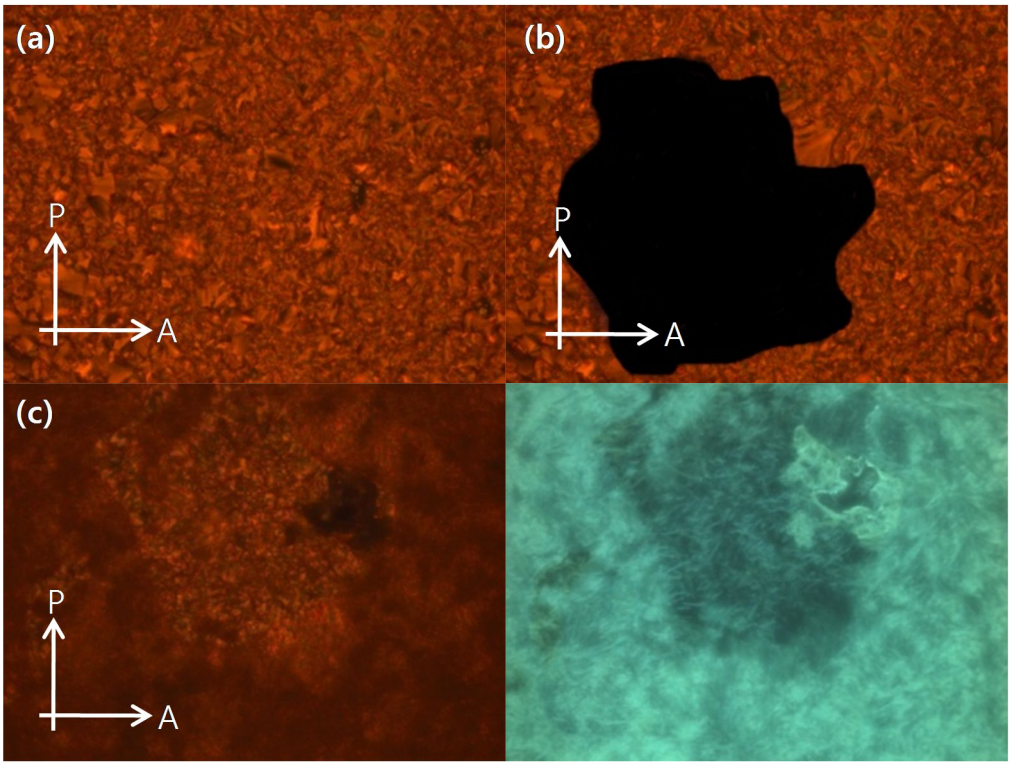

Figure 2.17. (a) The fan-shaped texture image in LC state of DDDCS at 150 °C. (b) Phase transition (smectic to isotroipic phase) by UV irradiation, (c) the image of crystal phase in cooling process, and (d) fluorescence image.

2.2.5. Demonstration of fluorescence patterning via photoisomerization behavior

As aleady discussed in a previous section, the fluorescence patterning experiment was conducted by using DDDCS material. The detailed experimental procedure is illustrated as shown in Figure 2.19. The thin film of DDDCS was prepared by spin-coating method (2000 rpm, 30 s). Then, thin film shows LC phase with increasing temperature by using hot-stage. The 365 nm UV irradiation in LC phase induces phase transition as shown in Figure 2.18b. Then, rapid cooling process (sample was quickly (1-2 sec) shifted from hotstage to the desk at RT) is introduced because we could not observe clear fluorescence patterns under slow cooling process.

Crystallization occured quickly and green colored fluorescence pattern was obtained as shown in Figure 2.20. The fluorescence patterning via photoinduced isomerization was perfectly demonstrated. The interesting issue of DDDCS material is the green fluorescence color of the film (Nanoparticles show blue color emission as shown above section). It means DDDCS molecule shows dual colored emission. It is similar phenomena as already reported in our group.[4c] Through this process, we could also demonstrate the dual colored fluorescence patterning by annealing process as shown in Figure 2.20. (green to blue phase) This emission process is caused by change of molecular stacking mode with external stimulus process.[4c]

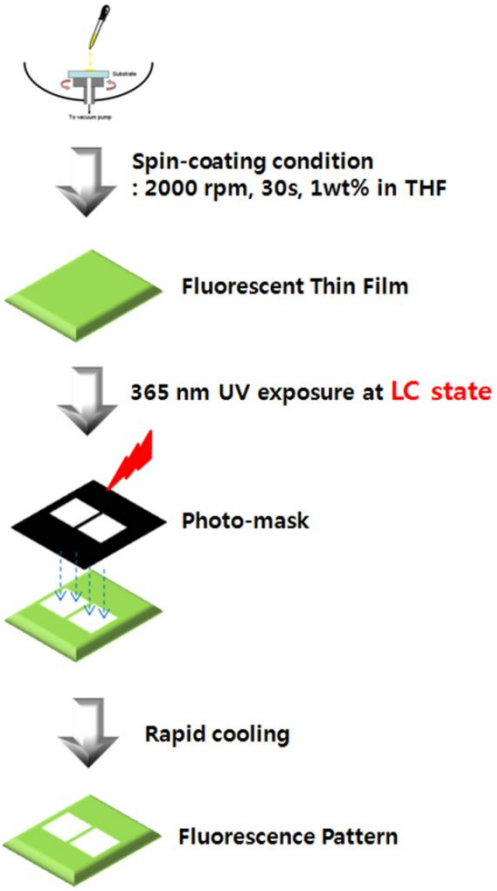

Figure 2.18. Experimental procedure for fluorescence patterning process.

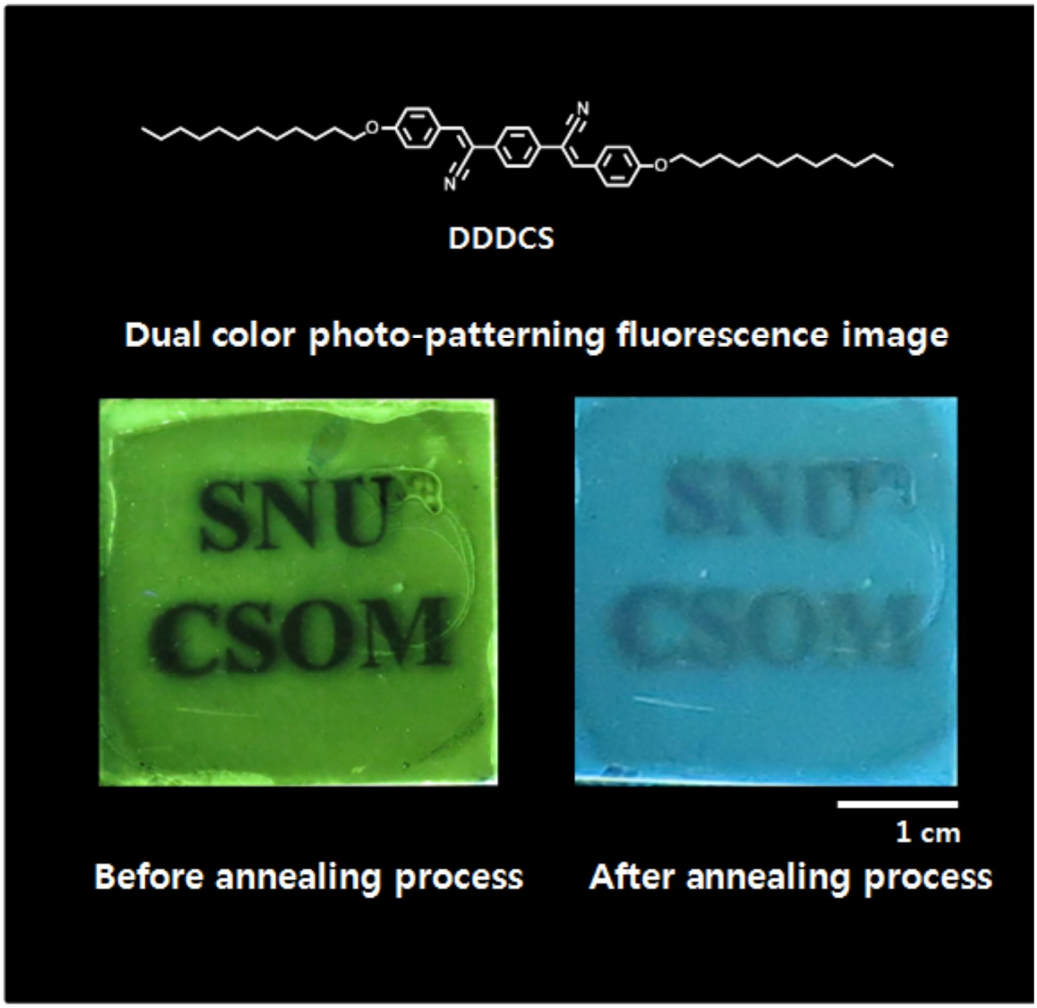

Figure 2.19. Dual colored fluorescence photo-patterning images of DDDCS via photoisomerization behavior. (left image: before annealing process, right image: after annealing process.)

2.3. Conclusion

We designed simple organic ∏–conjugated molecules based on cyanostilbene/dicyanodistrylbenzene type materials with various length of alkyl chain. Such molecules show AIEE behavior and LC formation due to self-assembly behavior with strong intermolecular secondary bonding. As the alkoxy length increases, LC phase changes from nematic to smectic phase. UV irradiation induces LC phase transition from nematic/smectic phase to isotropicphase due to photoinduced isomerization process. Through this process, we can perfectly demonstrate fluorescence patterning by using photo mask with UV irradiation. Furthermore, the different fluorescence color was shown by controling molecular stacking with external stimlus such as annealing process.

In this work, we firstly demonstrated fluorescence color patterning via photoinduced isomerization and change of molecular stacking in solid state based on cyanostilbene/DCS type materials. We believe this work will indicate a new class of soft materials in optical device application.

2.4. Experimental

2.4.1. General Information

Materials: All chemicals were purchased commercially, and used without further purification. Synthetic processes are described in the synthesis section.

Characterization: ^{1}H NMR spectra were recorded on a Bruker, Avance-300 (300 Mhz) in $CDCl_3$ solution. UV-visible absorption spectra were recorded on a Shimazu, UV-1650 PC spectrometer. Photoluminescence spectra were obtained using a Varian, Cary Eclipse Fluorescence spectrophotometer. The relative fluorescence quantum yield of solution and nanoparticles was measured using 9,10-diphenylanthracence (DPA) in benzene as a standard reference (1×10^{-4} mol L^{-1}, $\Phi_f = 0.83$). DSC measurements were made on a TA Instrument DSC Q 200. Light irradiation was performed with a hand-held lamp.

2.5. Bibliograrphy

1. (a) J. Zhang, J. K. Whitesell, M. A. Fox, *Chem. Mater.* **2001**, *13*, 2323; (b) S. Das, S. Varghese, N. S. S. Kumar, *Langmuir* **2009**, *26*, 1598; (c) J.-S. Yang, K.-L. Liau, C.-M. Wang, C.-Y. Hwang, *J. Am. Chem. Soc.* **2004**, *126*, 12325; (d) S. Menon, R. Thekkayil, S. Varghese, S. Das, *J. Polym. Sci., Part A: Polym. Chem.* **2011**, **49**, 5063; (e) T. Ubukata, S. Fujii, Y. Yokoyama, *J.Mater. Chem.* **2009**, 19.

2. (a) J. Gierschner, M. Ehni, H.-J. Egelhaaf, B. M. Medina, D. Beljonne, H. Benmansour, G. C. Bazan, *J. Chem. Phys.* 2005, *123*, 144914; (b) Z. Chen, U. Baumeister, C. Tschierske, F. Würthner*, Chem. Eur. J.* **2007**, *13,* 450.

3. (a) L. M. Goldenberg, V. Lisinetskii, Y. Gritsai, J. Stumpe, S. Schrader, *Adv. Mater.* **2012**, *24*, 3339; (b) L. H. Liu, K. Nakatani, R. Pansu, J. J. Vachon, P. Tauc, E. Ishow, *Adv. Mater.* **2007**, *19,* 433; (c) A. Jacquart, P. Tauc, K. Nakatani, E. Ishow*, J. Mater. Chem.* **2009**, *19*, 8999; (d) S. Wu, X. Yu, J. Huang, J. Shen, Q. Yan, X. Wang, W. Wu, Y. Luo, K. Wang, Q. Zhang, *J. Mater. Chem.* **2008**, *18*, 3223.

4. (a) B.-K. An, J. Gierschner, S. Y. Park, *Acc. Chem. Res.* **2011**, *45*, 544; (b) B.-K. An, S.-K. Kwon, S.-D. Jung, S. Y. Park, *J. Am. Chem. Soc.* **2002**, *124*, 14410. (c) S.-J. Yoon, J. W. Chung, J. Gierschner, K. S. Kim, M.-G. Choi, D. Kim, S. Y. Park, *J. Am. Chem. Soc.* **2010**, *132*, 13675; (d) S.-J. Yoon, J. H. Kim, K. S. Kim, J. W. Chung, B. Heinrich, F. Mathevet, P. Kim, B. Donnio, A.-J. Attias, D. Kim, S. Y. Park, *Adv. Funct. Mater.* **2012**, *22*, 61.

5. (a) A. Gulino, F. Lupo, G. G. Condorelli, M. E. Fragala, M. E. Amato, G. Scarlata, *J. Mater. Chem.* **2008**, *18*, 5011; (b) L. Zhu, C. Y. Ang, X. Li, K. T. Nguyen, S. Y. Tan, H. Ågren, Y. Zhao, *Adv. Mater.* **2012**, *24*, 4020.

6. (a) J. W. Goodby, D. W. Bruce, M. Hird, C. Imrie, M. Neal, *J. Mater. Chem.* **2001**, *11*, 2631; (b) I. W. Hamley, *Angew. Chem.* **2003**, *115*, 1730; (c) M. D. Hollingsworth, *Science* **2002**, 295, 2410.

Chapter 3. Highly Fluorescent micro patterns via phototriggered mass migration behavior in cyanostilbene-based crystalline thin film

3.1 Introduction

Azobenzene functionalized polymers have been intensively investigated during past few decades due to their successful applications in optoelectronics such as optical memory devices, optical switchings, sensors and diffractive optical elements.[1] In azobenzene-containing film, the irradiaton of the polarized light of appropriate wavelength causes an efficient trans-cis photoisomerization of azobenzene and a photoinduced reorientation of molecules at the molecular level, leading to a mass migration at the micrometer level.[1a,b] As a result of the mass migration, the surface relief grating (SRG) structure is readily formed in amorphous azobenzene film. For the last several decades, this class of photoinduced SRG induced by the interfering laser beam had been widely demonstrated in a various types of azobenzene-containing amorphous polymers, liquid crystalline (LC) polymers, and high-T_g organic glasses.[2] However, more exploration for fully understanding of this type of SRG mechanism is still required. Another class of SRG based on the phase transition had been proposed by Seki *et al*.[3] They have reported the phototriggered SRG of smetic A LC polymer containing azobenzene accompanying the phase transition from LC to isotropic upon illumination independent of polarization. Such a phase transition originated from a photoisomerization of azobenzene without temperature variation. The induced isothermal two phases have a considerable disparity in viscosity and surface tension at their interfaces, resulting in an effective mass migration under a small photon dose (~100 mJ/cm^2). With respect to molecular design for the phototriggered mass migration, it

is essential that the thermotropic behavior of LC materials containing azobenzene mesogen is coupled with the photo-assisted phase transition.

Recently, these SRG techniques utilizing photoactive azobenzene materials as a simple and single-step patterning fabrication method, have been successfully employed to develop the fluorescence micropattern by adding of a fluorescent dye into azobenzene material matrix.[4] Nevertheless, at the current stage, there are only a few reports to be successfully demonstrated, because of the following limited requirements for optical applications: 1) a high fluorescence quantum yield in solid film and 2) a spectral separation between the emission of fluorophore and the absorbance of azobenzene dye for the frustrated Förster-type energy transfer between them.

To date, we have reported a novel class of α-cyano-substituted stilbenic derivatives exhibiting a unique and peculiar fluorescence behavior, that is, aggregation-induced enhanced emission (AIEE): it is virtually non-fluorescent in the monomer state in solution but becomes highly fluorescent upon self-assembly into supramolecules.[5] This phenomenon is attributed to a torsional motion of a cyanostilbene moiety that has a local dipole moment in a perpendicular direction to the long axis of the molecule, inducing a dipole-dipole interaction in the neighbored stacked molecules with an antiparallel fashion. Upon aggregation, the planarization of a cyanostilbene unit causes π-π interaction of the extended π-conjugated aromatics. At the same time, it works with the secondary interactions such as CH---π and CH---N upon a self-assembly, leading to the specific tight stacking and the enhanced solid-state fluorescence.[5b] Furthermore, typical AIEE molecules with the cyanostilbene unit are able to undergo a trans-cis photoisomerization, as commonly observed in stilbene and azobenzene materials.[6] Such a photoisomerization process is considered to have an important role in the formation of SRG via a mass migration. However, among cyanostilbene-containing materials, there is no report on the SRG application, so far, unlike photoisomerizable azo-containing materials.

Very recently, we have presented a new dicyanodistyrylbenzene-based phasmidic molecule exhibiting a columnar hexagonal LC at room temperature, together with a strong thermochromic luminescence due to the mesomorphic orientation in LC and solid crystalline state.[5d] As mentioned earlier, the phototriggered mass migration could be strongly coupled with a mesomorphic behavior of trans- and cis-isomer, inducing the phase transtion upon the photoisomerization. In this respect, herein, we have designed and synthesized a simple hexacatenar-type AIEE molecule consisting of cyanostilbene and flexible tris(dodecyloxy) group, showing a columnar hexagonal phase that is transformed into tetragonal packing crystals under slow cooling at RT. The resulting crystalline film also exhibited a rapid and clear phase transition from crystalline to LC phase upon a trans-cis photoisomerization during UV irradiation at the critical processing temperature. In this chapter, we have presented a new concept of cyanostilbene-containing thermotropic molecules that undergo the apparent phototriggered mass migration from LC region to crystalline one, leading to crystallization-induced fluorescence patterning in crystalline film.

Cyanostilbene-based hexacatenar liquid crystal studied in this present work, (Z)-2,3-bis(3,4,5-tris(dodecyloxy)phenyl)acrylonitrile (GCS) was synthesized by Knoevenagel reaction of 3,4,5-tris(dodecyloxy)benzaldehyde and 2-(3,4,5-tris(dodecyloxy)phenyl)acetonitrile in a good yield. (See Scheme 3.1)

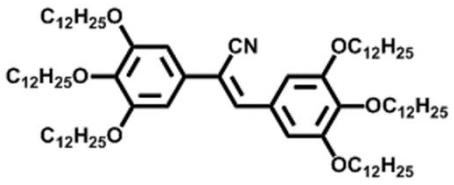

Scheme 3.1. Chemical structure of GCS.

3.2. Results and discussion

3.2.1. Synthesis

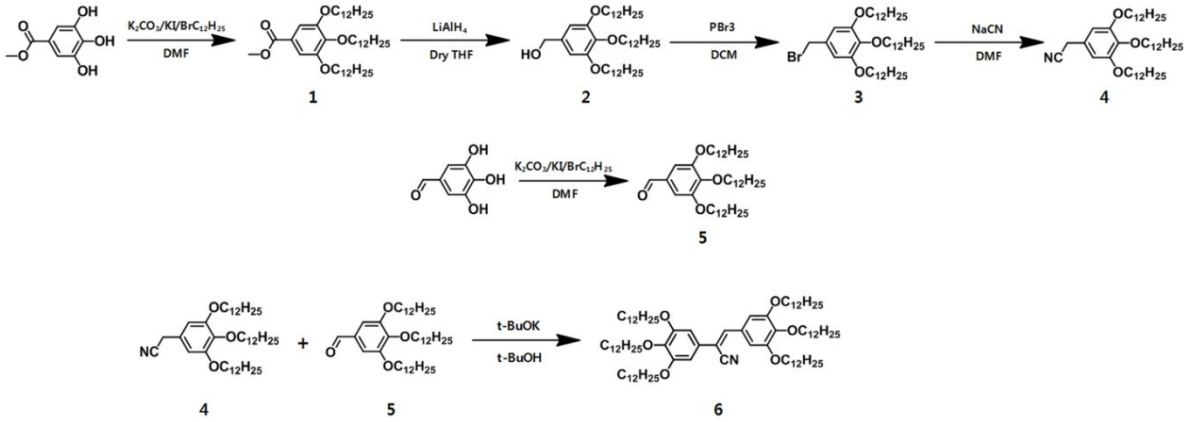

Scheme 3.2. Synthetic scheme of GCS.

Methyl 3,4,5-tris(dodecyloxy)benzoate (1).

K_2CO_3 (9.01 g, 76 mmol) and KI (catalytic amount) were added to a solution of methyl 3,4,5-trihydroxybenzoate (3.5 g, 19 mmol) in dry DMF (15 mL), and the mixture was stirred at 80 °C. 1-Bromo-dodecane (15.63 mL, 76 mmol) was slowly dropped into the mixture. The reaction lasted overnight. After cooling to room temperature, the mixture was poured into brine and extracted with dichloromethane. The organic phase was dried over $MgSO_4$ and the solvent was evaporated *in vacuo*. The product (12.5 g, 96 %) was obtained by column chromatography using ethyl acetate and n-hexane (1:10 v/v). **^{1}H NMR** (300 MHz, $CDCl_3$, δ): 7.27 (s, Ar-H, 2H), 4.02 (m, 6H, -OCH_2), 3.90 (s, 3H, -OCH_3), 1.79 (m, 6H, -CH_2), 1.45 (m, 6H, -CH_2), 1.27 (m, 48H , -CH_2), 0.88 (t, 9H, -CH_3)

(3,4,5-tris(dodecyloxy)phenyl)methanol (2).

A stirred suspension of $LiAlH_4$ (0.7 g, 18.14 mmol) in dry THF (15 mL) was added dropwise to

a solution of **1** (10 g, 14.51 mmol) in THF (25 mL) at 0 °C. After stirring for 12 h at room temperature, the reaction mixture was quenched with a small amount of methanol and water. The insoluble materials were filtered off, and the filtrate was concentrated under a reduced pressure. The residue was dissolved in $CHCl_3$, washed with water and brine, and dried over $MgSO_4$. After filtration and evaporation, the product (8.81 g, 92%) was obtained by reprecipitation from CH_2Cl_2 and methanol solution. **^{1}H NMR** (300 MHz, $CDCl_3$, δ): 6.55 (s, Ar-H, 2H), 4.6 (d, 2H, -OCH_2), 3.95 (m, 6H, -OCH_3), 1.79 (m, 6H, -CH_2), 1.45 (m, 6H, -CH_2), 1.27 (m, 48H, -CH_2), 0.88 (t, 9H, -CH_3)

5-(bromomethyl)-1,2,3-tris(dodecyloxy)benzene (3).

a solution of PBr3 (2.5 mL, 26.32 mmol) in CH_2Cl_2 (10 mL) at 0 °C was added a stirred solution of **2** (8.7 g, 13.16 mmol) in CH_2Cl_2 (100 mL). The mixture was allowed to react for 3 h at room temperature, and then poured into a large amount of water. The product was extracted with $CHCl_3$ three times. The combined organic layers were washed with brine, and dried over $MgSO_4$. After filtration and evaporation, the product (9.3 g, 98 %) was dried under a reduced pressure to give **3** as a white powder. **^{1}H NMR** (300 MHz, $CDCl_3$, δ): 6.57 (s, Ar-H, 2H), 4.4 (s, 2H, -OCH_2), 3.95 (m, 6H, -OCH_3), 1.79 (m, 6H, -CH_2), 1.45 (m, 6H, -CH_2), 1.27 (m, 48H, -CH_2), 0.88 (t, 9H, -CH_3)

2-(3,4,5-tris(dodecyloxy)phenyl)acetonitrile (4).

3 (9.3 g, 13.16 mmol) was added into a slurry of sodium cyanide (NaCN, 1.3 g, 26.32 mmol) in dry DMF (50 mL), and stirred at 45 °C for 3 days. After cooling to room temperature, the mixture was poured into brine, and the resulting precipitate was filtered. The product (6.09 g, 71 %) was obtained by column chromatography using ethyl acetate and n-hexane. **^{1}H NMR** (300 MHz, $CDCl_3$, δ): 6.47 (s, Ar-H, 2H), 3.95 (m, 6H, -OCH_3), 3.65 (s, 2H, -OCH_2), 1.79 (m, 6H, -CH_2), 1.45 (m, 6H, -CH_2), 1.27 (m, 48H, -CH_2), 0.88f (t, 9H, -CH_3)

3,4,5-tris(dodecyloxy)benzaldehyde (5).

K_2CO_3 (2.9 g, 21 mmol) and KI (catalytic amount) were added to a solution of 3,4,5-trihydroxybenzaldehyde (1 g, 5.81 mmol) in dry DMF (15 mL), and the mixture was stirred at 80 °C. 1-Bromo-dodecane (6.95 mL, 29 mmol) was slowly dropped into the mixture. The reaction lasted overnight. After cooling to room temperature, the mixture was poured into brine and extracted with dichloromethane. The organic phase was dried over $MgSO_4$ and the solvent was evaporated *in vacuo*. The product (1.8 g, 47 %) was obtained by column chromatography using ethyl acetate and n-hexane (1:10 v/v). **^{1}H NMR** (300 MHz, $CDCl_3$, δ): 9.83 (s, 1H, -CHO), 7.08 (s, Ar-H, 2H), 4.04 (m, 6H, $-OCH_3$), 1.79 (m, 6H, $-CH_2$), 1.48 (m, 6H, $-CH_2$), 1.27 (m, 48H, $-CH_2$), 0.88 (t, 9H, $-CH_3$)

(Z)-2,3-bis(3,4,5-tris(dodecyloxy)phenyl)acrylonitrile, GCS (6).

The mixture of **4** (0.31 g, 0.46 mmol) and **5** (0.3 g, 0.46 mmol) in tert-butyl alcohol (15 mL) was stirred at 50 °C. Potassium tert-butoxide (0.05 g, 0.46 mmol) powder was dropped into the mixture and sitred for 2 h. The resulting precipitate was filtered and purified by column chromatography using dichloromethane. GCS bulk powder (0.4 g, 67 %) was obtained by reprecipatiation from dichloromethane and methanol solution. **^{1}H NMR** (300 MHz, $CDCl_3$, δ) : 7.28 (s,1H, Vinyl), 7.12 (s, 2H, Ar-H), 6.8 (s, 2H, Ar-H), 4.05(m, 12H, $-OCH_2$), 1.79 (m, 12H, $-CH_2$), 1.48(m,12H, $-CH_2$), 1.27(m, 96H, $-CH_2$), 0.88(t, 18H, $-CH_3$) **^{13}C NMR** (500 MHz, $CDCl_3$) δ[ppm]: 153.50, 153,20, 141.59, 129.90, 128.68, 118.54, 110.08, 107.98, 104.92, 73.63, 69.47, 69.31, 31.93, 30.37, 29.75, 29.71, 29.65, 29.61, 29.43, 29.37, 26.13, 22.69, 14.09 **m/z (FAB+ MS)** Calcd for $C_{87}H_{155}NO_6$, 1311.1933; Found, 1311.1937. EA Anal. Calcd for $C_{87}H_{155}NO_6$: C, 79.69; H, 11.92; N, 1.07; O, 7.32 . Found: C, 79.50; H, 11.94; N, 1.09; O, 7.39.

3.2.2. Liquid crystal & crystallization property

From a viewpoint of the molecular structure for LC, the cyanostilbene core with a local dipole-dipole interaction and a photoisomerization function, is directly attached by peripheral flexible side chain of tris(dodecyloxy) group that can facilitate a mesomorphic organization and provide a free volume for photoisomerization.[5d] The mesogenic behavior of GCS was evaluated using differential scanning calorimetry (DSC), polarized optical microscopy (POM), and X-ray diffraction (XRD), as shown in Figure 3.1a,b. The DSC traces showed the phase-transition temperature and associated enthalpy values of GCS (See Figure 3.1a). As shown in Figure 3.1b of POM image, the typical focal-conic fan-shaped texture was observed at ca. 30 °C in the cooling process, clearly indicating a formation of a columnar hexagonal (Col_h) phase. As shown in Figure 1c, the scattering profile of the GCS displayed several major diffraction peaks at the small angle of 24.8, 14.2, 12.4 Å corresponding to layer spacing in the ratio of 1, $(1/3)^{1/2}$ and 2. They were clearly assigned to (100), (110) and (200) in the two-dimensional hexagonal lattice (a = 28.6 Å) with *p6mm* symmetry, respectively. However, this mesophase could not remain the same phase on a slow cooling from 30 ^{o}C, unlike supercooling process in DSC. It accompanied a partial crystallization at near RT. Thus, a columnar hexagonal LC phase was promptly transferred to crystalline phase at 26^{o}C. As shown in Figure 3.1d, the small angle peaks due to long range periodicity were observed at 23.99, 16.92 and 11.44 Å. These peaks were assigned to the layer spacing ratio of 1, $(1/2)^{1/2}$ and 2, indicating a highly ordered crystalline phase in the tetragonal arrangement. In general, for discotic LC molecules, the interplay and balance of a rigidity of disk-type core and a flexibility of a multiple terminar alkyl side chain strongly affect a stabilization of columnar LC phase. The temporal mesophase stability of GCS at near RT has a kinetically limitation driven by intermolecular forces like strong π-π interaction, dipole-dipole interaction, hydrogen bonding and van der Waals force *etc*. As a result, GCS molecules have a strong tendency to form a crystalline phase in tetragonal arrangement via LC mesophase at near RT.

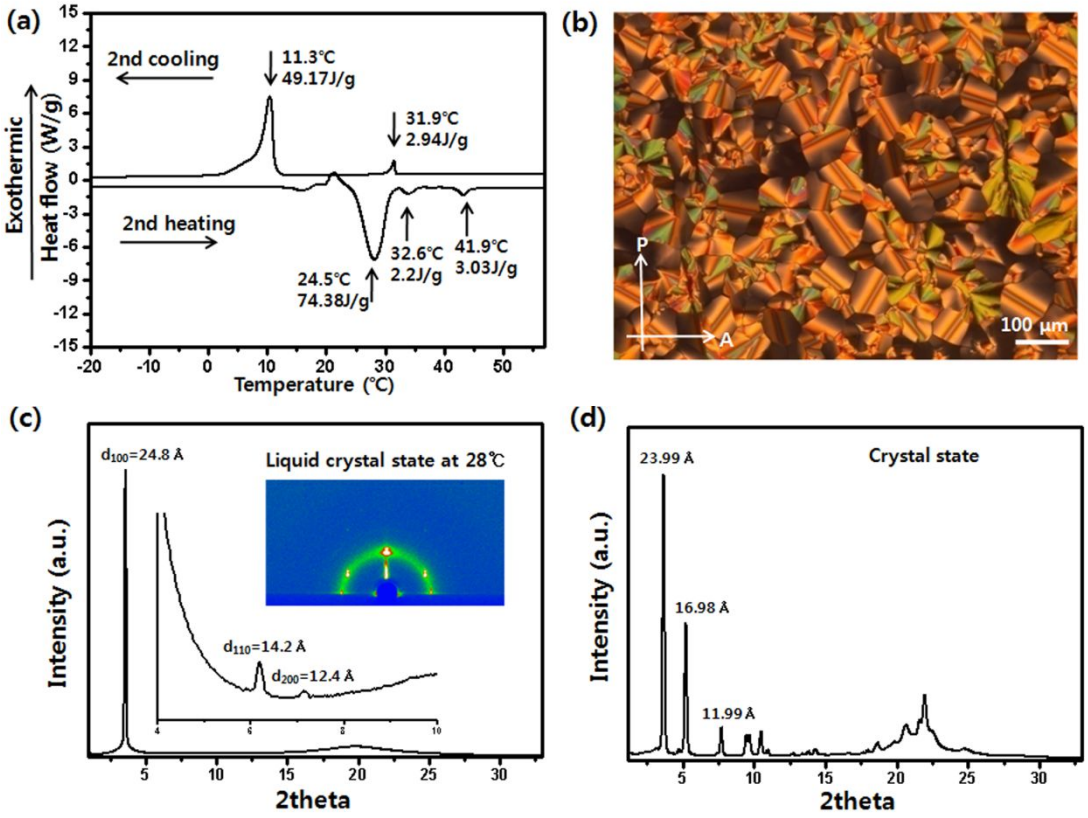

Figure 3.1. (a) DSC trace of GCS on heating/cooling rate of 5 °C per minute, (b) The Col_h liquid crystal phase obtained in POM at 30 °C on the cooling process. XRD pattern of GCS LC phase at 28 °C (c), and crystal phase(d). Inset in (c) showed the magnified diffraction peaks and 2D pattern image.

3.2.3. Formation of soft crystalline film

We prepared a thin film through a spin-coating (2000 rpm, 30 s) using a chloroform solution of GCS (3 wt%). The thickness of the obtained film was 400 nm as evaluated by the atomic force microscopy (AFM). Initially, as-prepared film looks like amorphous state with a high transparency. However, a partial crystallization in the film occurs subsequently. During overnight under dark at near RT (25~30 ^{o}C), it was transformed into the perfectly uniform crystalline film that had the same tetragonal crystal arrangment to the GCS bulk powder. (See Grazing-incidence XRD (GI-XRD) pattern of Figure 3.2**)** However, it was noted that the resulting crystalline film has much less ordered packing than that of the GCS bulk powder, probably due to much broader diffuse halo without apparent specific peaks in a wide angle region of GI-XRD pattern as well as a relatively low intensity of the diffraction peaks in a small angle. Furthermore, even increasing temperature, we could not observe LC state, only see crystal to isotropic phase transition, which means tetragonal packing is more stable than hexagonal packing in GCS crystalline state. (See Figure 3.3)

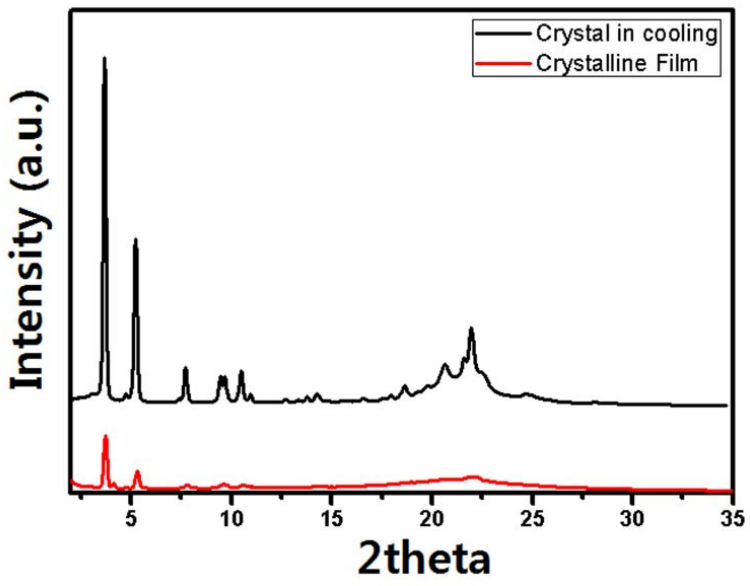

Figure 3.2. 2D XRD patterns of the crystal phase of GCS in cooling process and crystalline film of GCS.

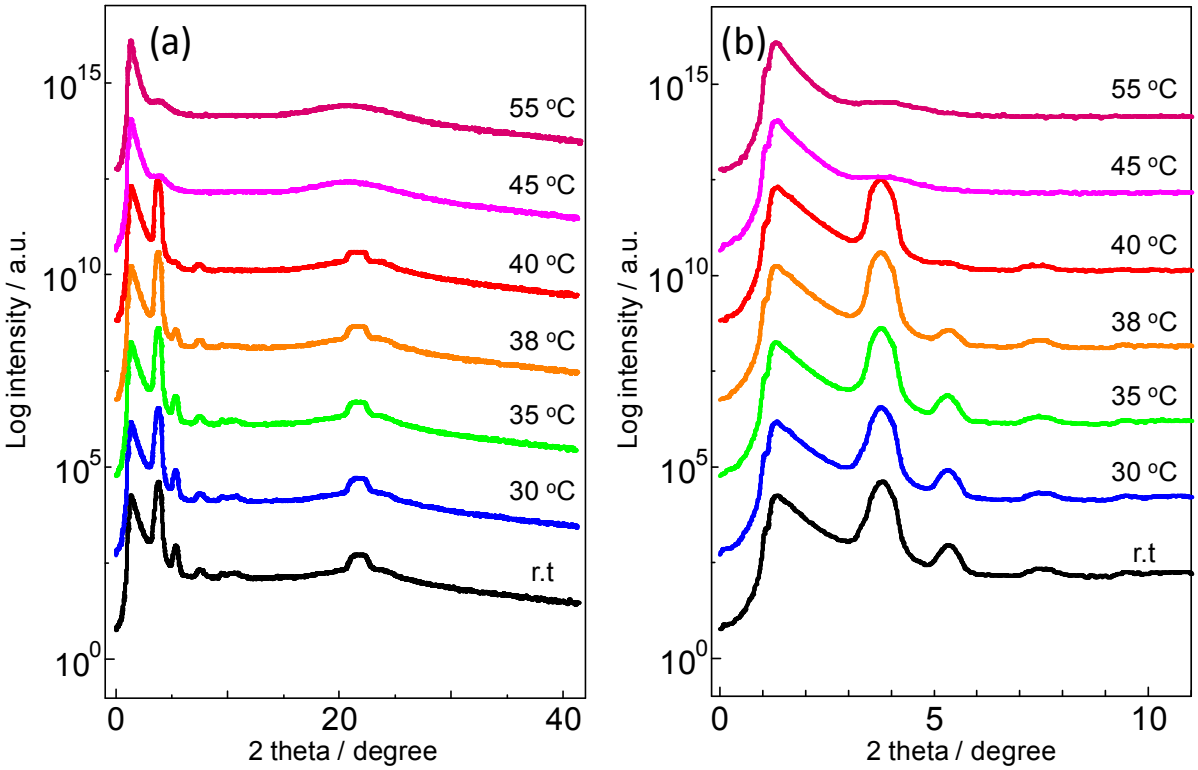

Figure 3.3. Log-scaled 2D GI-XRD patterns of the initial crystalline film of trans-GCS before UV irradiation depending on the temperature, in the wide angle (a) and the small angle regions (b).

3.2.4. Aggregation induced enhanced emission (AIEE) behavior

We have studied the optical and fluorescent characteristic of GCS molecule in solution and film. As shown in Figure 3.4a, the π-π* transition absorption of GCS was observed at 357 nm in THF solution (2 x 10^{-5} M). In crystalline film, it showed a hypsochromic shift by only ~8 nm, implying a formation of weakly bound H-type aggregates. Nevertheless, GCS exhibited strong solid-state fluorescence, unlike common fluorescent dye accompanying a concentration quenching.[7] As shown in Figure 3.4b, the virtually no fluorescence was observed in THF solution (Φ_F = 0.006) while strong blue emission centered at 467 nm was appeared in crystalline film state (Φ_F = 0.22). Such a PL behavior was in agreement with a typical AIEE characteristic. Time-resolved fluorescence lifetime experiments conducted by the time-correlated single-photon-counting (TCSPC) technique also supported this trend. (See Table 3.1) In crystalline film, fluorescence lifetime of 2.54 ns was much larger than negligible one (<80 ps, instrument response limit) in THF solution, which can be clearly explained by our previous studies on the correlation between molecular conformation and photophysical property as follows:[5a] the optimized geometry of the cyanostilbene based molecule corresponded to a twisted conformation in the isolated monomer state. Such a torsional motion of the cyanostilbene involved in the main pathway of non-radiative deactivation from the excited state, gave rise to almost no fluorescence. In crystalline film, the discotic mesogen of the cyanostilbene aromatics of GCS stacks in a weakly bound H-type fashion along column in a tetragonal crystal arrangement. This aggregation induced the planarization of the cyanostilbene unit, together with its restricted intramolecular rotational motion. Rather than concentration quenching, it resulted in a large enhancement by 37 times in fluorescence for crystalline film, by reducing non-radiative deactivation pathway.

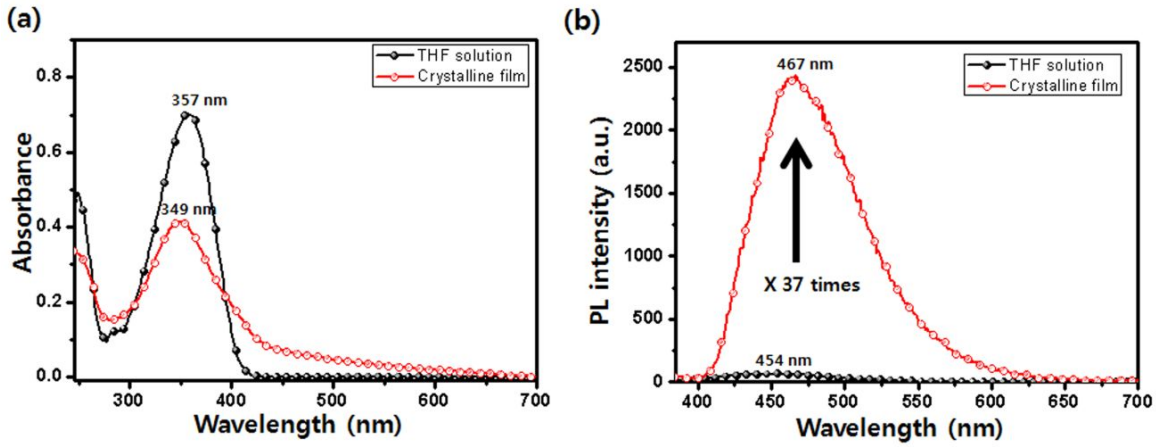

Figure 3.4. UV-visible absorption (a) and photoluminescence (b) spectra of GCS in THF solution ($c = 2 \times 10^{-5}$ mol L^{-1}, filled black circle), crystal film (open red circle).

Table 3.1. Photophysical properties of GCS in THF solution and crystalline film

Phase	λ^{max}_{abs} [nm]	λ^{max}_{em} [nm] [a]	Φ_f	τ_{av} [ns]
Solution	357	454	0.006	N.D.[b]
Crystal	349	467	0.22	2.54

[a] λ_{exc} = 360 nm. [b] N.D. = Not determined

3.2.5. Photo-induced isomerization behavior

3.2.5.1. Solution state

Another function of the cyanostilbene unit of GCS is the photoinduced trans-cis isomerization. As shown in Figure 3.5a, we observed UV-visible absorption spectra of the solution state of GCS (2×10^{-5} M) according to UV light irradiation, which promoted the trans to cis photoisomerization. Upon irradiation with the 365 nm UV (1 mW cm^{-2}), the absorption band at 357 nm of trans-GCS decreased and new absorption peak bands at 244 and 288 nm appeared with one isosbestic point at 326 nm. The generated cis isomer exhibited a blue-shift in the absorption wavelength as compared to trans isomer because of the reduced effective conjugation length of the bent conformation.[8] The photo-stationary state (PSS) was reached in about 50 s in solution. From ^{1}H NMR spectroscopy of Figure 3.5b,c, the resulting conversion ratio of tran to cis is estimated to correspond to 60 ± 1 % at photostationary equilibrium state.

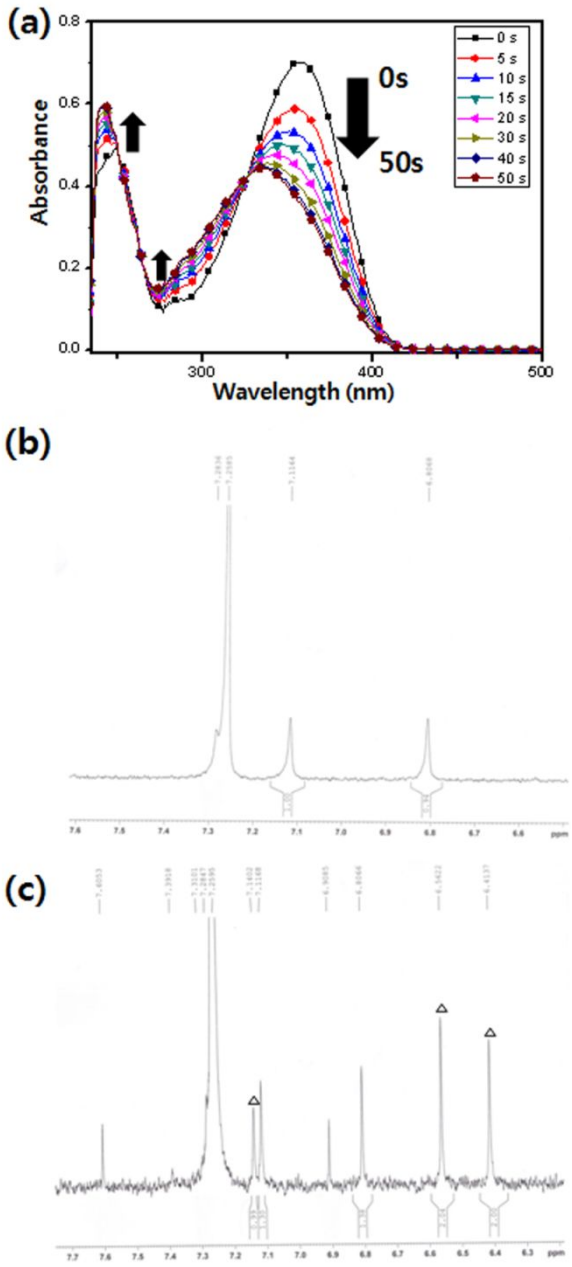

Figure 3.5. (a) Photoisomerization behavior of GCS in THF solution (2×10^{-5} M): changes the UV-vis absorption spectra during 365 nm UV light (1 mW cm^{-2}) irradiation at room temperature. (b) ^{1}H NMR spectra (300 MHz, $CDCl_3$, 298 K) of GCS before UV irradiation (c) after UV irradiation (△: cis form).

3.2.5.2. Crystalline state

To control photo-induced isomerization behavior in crystalline state, we observed change of UV-visible absorption spectra with UV irradiation on the crystalline state at RT as shown in Figure 3.6a. Befor UV irradiation, for RT, a broad absorption tail in the long wavelength range was observed probably due to the scattering of the crystalline film. Furthermore, after the initial irradiation, a decrease of absorption at 349 nm in UV-visible absorption spectra was observed. However, after another irradiation (1~2 min) for about 3 min, phase transition was induced. It means the photo-induced isomerization behavior could not occur at RT. Therefore, it implies that the photoisomerization in film at RT is not efficient for further mass migration. In order to get more less packing and soft crystalline state, we investigated the crystalline film at near 38 ^{o}C, without destroying crystalline state. As expected, in contrast to RT, the absorption tail became weakened significantly at near 38 ^{o}C. Just after the initial irradiation (within several seconds), the phase transition occurred promptly. The π-π^* transition absorption of trans-GCS at 349 nm showed a substantially decreasing behavior without some barrier, together with a increase in absorption intensity at the short wavelength due to the higher conversion of cis form from trans one. The presence of one isosbestic point at 285 nm also implies that any other photochemical reaction like photo-bleaching is most probably to be excluded during the short time-irradiation (within 2~3 mins). Thus, it resulted in an efficient photoisomerization at near 38 ^{o}C. For the in-depth fundamental understanding of photo-isomerization behavior in crystalline state, we have observed optical texture change by using POM with UV irradiation as a function of time at RT and about 38 °C (See Figure 3.7). In case of an irradiation at RT, the phase transition in the irradiated region was observed within several minutes, followed by a considerable decrease in emission. To elucidate on the phase-transition state, we have measured the GI-XRD data. As shown in Figure 3.8, GI-XRD result of the irradiated film revealed the phase change of GCS from tetragonal-like crystal to Col_h phase that has the diffraction peaks at 23.99, 14.52, 12.30 Å corresponding to the characteristic ratio of 1, $(1/3)^{1/2}$ and 2 for hexagonal packing. This Col_h

phase of GCS in PSS state is not identical to that observed in trans-GCS. Such a phase transition originated from the accumulation of the cis isomer upon photoisomerization inducing a loose packing, followed by breaking a crystal structure. As discussed in Figure 3.2 (low-intensity diffraction peak in a small angle and a broad diffuse halo with no specific peak in a wide angle), the crystalline film is considered to have a reduced crystalline periodic lattice with a partial disorder via weaker intermolecular interaction, with respect to perfect crystal packing the GCS bulk powder. Thus, GCS may be able to undergo trans-cis isomerization within some free volume even though the crystalline structure. But, a much longer time-irradiation is needed as compared to the solution state where the PSS was reached in about 50 s. Moreover, even after an irradiation for 30 min, mass migration is not completed from irradiated area to dark area. Unlike the case at RT, when exposed UV light at near 38 °C, the crystalline film exhibited the much faster phase transition (to Col_h phase) and completed the phototriggered mass migration within 90 sec as shown in Figure 3.7b. As shown in Figure 3.8, after sufficient UV irradiation, the crystalline phase was observed to finally change into another columnar hexagonal phase, regardless of the operating temperature. It means that under the thermally activated state, higher accumulation of the cis-GCS by the effective photoisomerization at early UV irradiation can facilitate a fast transition from a hard crystal to a soft matter of LC phase at near 38 °C, which has a lower viscosity and a less ordering than the one at RT,[9] and thus, has a sufficient mobility for mass transport toward non-irradiated area via diffusivity without any other thermal phase transition.[10]

We could demonstrate possibility of the surface and fluorescence patterns through such process.

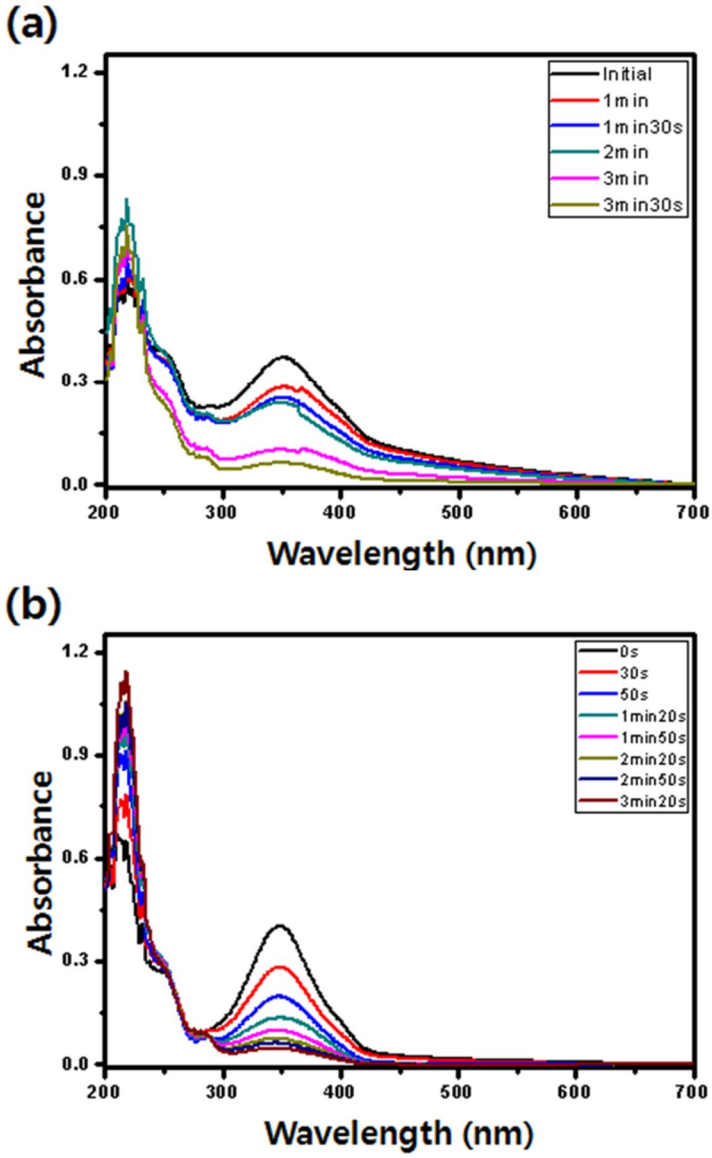

Figure 3.6. The UV-vis absorbance spectra as a function of UV irradiation time in GCS crystalline film at (a) RT and (b) 38 °C.

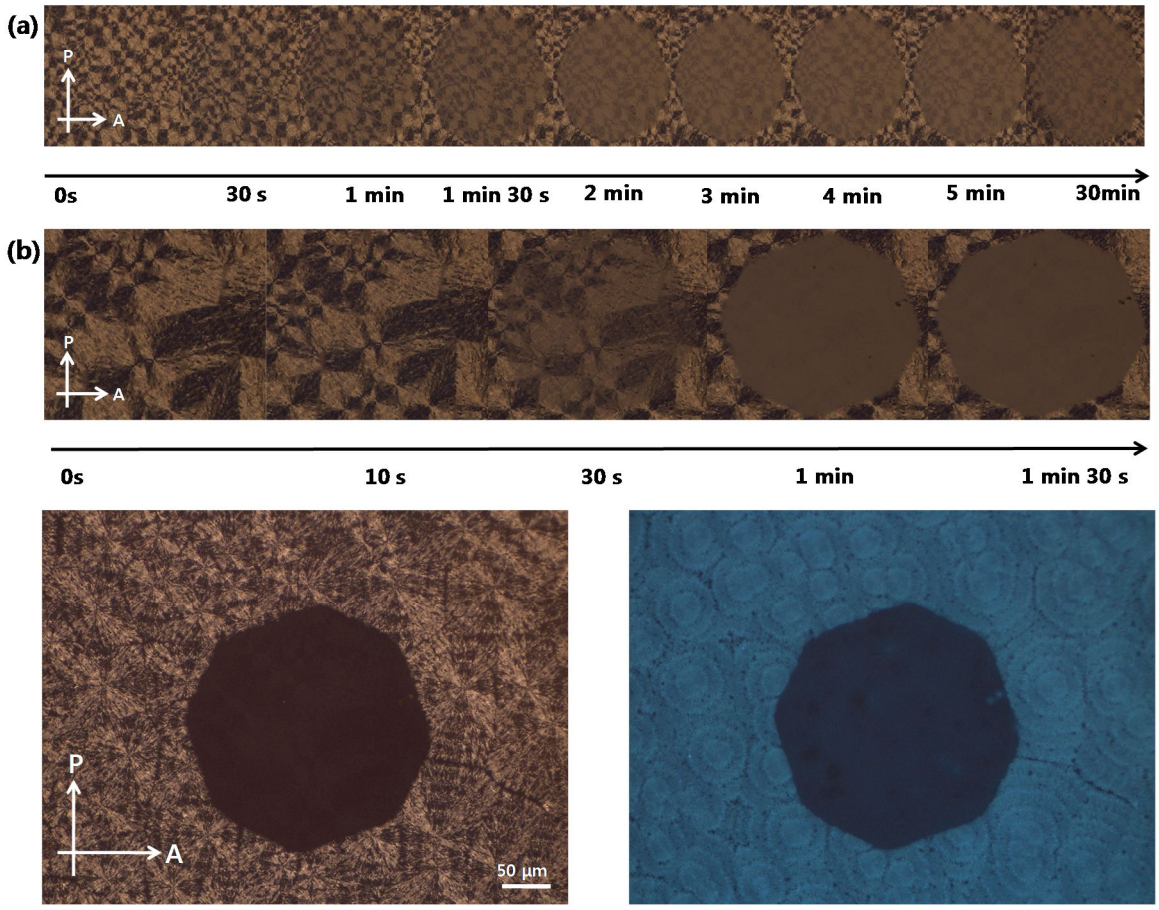

Figure 3.7. Photoinduced isothermal phase transition on the crystalline state of GCS at (a) RT, and (b) near 38 °C.

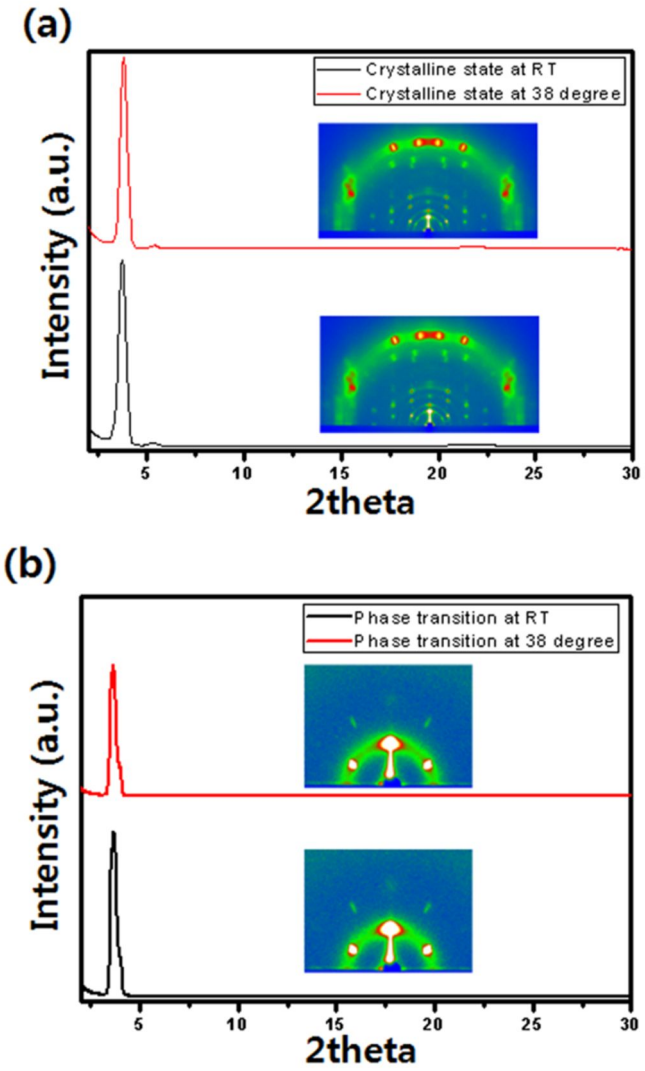

Figure 3.8. 2D GI-XRD patterns of the (a) initial crystalline state at RT and 38 °C, (b) phase transition state with UV irradiation at RT and 38 °C.

3.2.6. Highly fluorescent micro patterns via phototriggered mass migration behavior in cyanostilbene-based crystalline thin film

We performed the phototriggered surface relief grating experiment as shown in Figure 3.9. By following the experimental procedure of the phototriggered mass migration on the principle of the phase transition type,[3] we exposed non-polarized Hg lamp at 365 nm (1 mW cm^{-2}) on the crystalline film through the micropatterned-photomask (10 μm line and space patterns) at near 38 °C. The formation of surface relief structures was monitored as function of photon dose by measuring the first order diffraction efficiency using Helium-Neon (He-Ne) laser (See Figure 3.10a). The diffraction efficiency had an increasing trend as the light energy increases, and then was saturated to 29.4 % at 150 mJ cm^{-2}. When exposed higher than 150 mJ cm^{-2}, it showed a decreasing behavior as photo-bleaching of cyanostilbene moiety may occur under high energy-irradiation as shown in Figure 3.11. It is noteworthy mentioning that the diffraction efficiency of almost 30% even at a small photon dose is comparable to that previously reported in azobenzene-containing materials applicable to SRG fabrication.[2] The resulting SRG structure was directly observed by AFM images, exhibiting clear and typical modulation of the surface on the crystalline film. (See Figure 3.10b). The spatial period of the patterns was coincident with that of the photomask. Its depth from peak to trough (Δh) was about 823 nm, resulting in nearly 200 % modulation efficiency. Quite interestingly, the phototriggered mass migration of GCS is so remarkably efficient in the crystalline film. It is probably acceptable that the cyanostilbene unit of GCS works effectively for SRG structure like the azobenzene unit demonstrated in the well-studied system for SRG.[2] At the same time, highly fluorescent micropatterns with high contrast were simply developed as displayed in a fluorescence optical microscopy of Figure 3.10c. It was noted again that this cyanostilbene-based molecule in solid crystalline film exhibited an inherent AIEE behavior and strong blue fluorescence without concentration quenching which occurred in most of fluorescent materials. (*vide infra* for the detailed

discussion of fluorescent characteristic of GCS) Thus, our approach in this work is totally different from a combined system by embedding fluorescent chromophore into a photoisomerization-active azobenzene material as mentioned in the beginning. To the best of our knowledge, we believe that the present work is the first example to demonstrate highly fluorescent micropattern based on the phototriggered mass migration in the crystalline film of a cyanostilbene-type fluorescent material.

Furthermore, to gain a more insight into the formation of SRG of the film, we carried out UV light irradiation experiment under the same condition as discussed above, using a different photomask with "3" character-shape. As shown in Figure 3.10e, it was clearly observed that the mass migration from the irradiated region in the film to the shaded region took place. So, it caused the highest depth modulation at the boundary of the irradiated region from "3" character-shape.

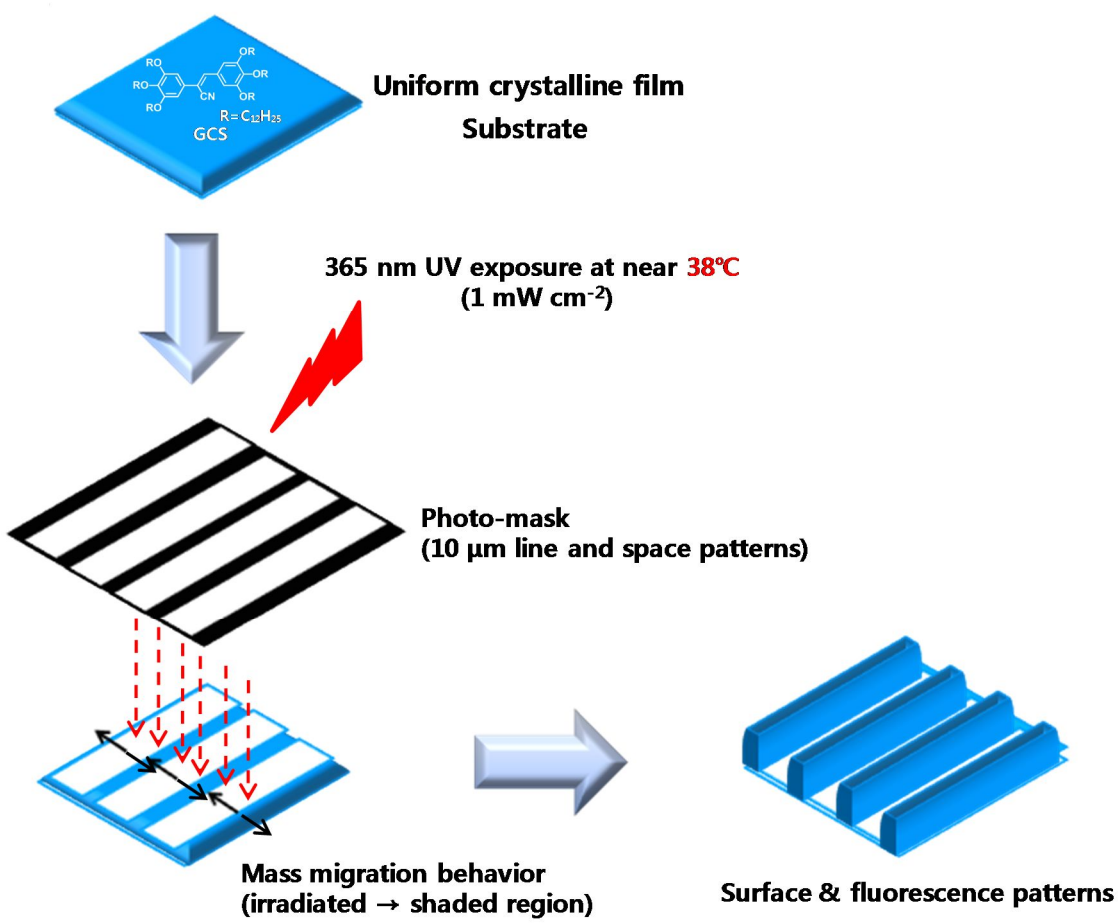

Figure 3.9. The experimental procedure for high fluorescent micro patterns.

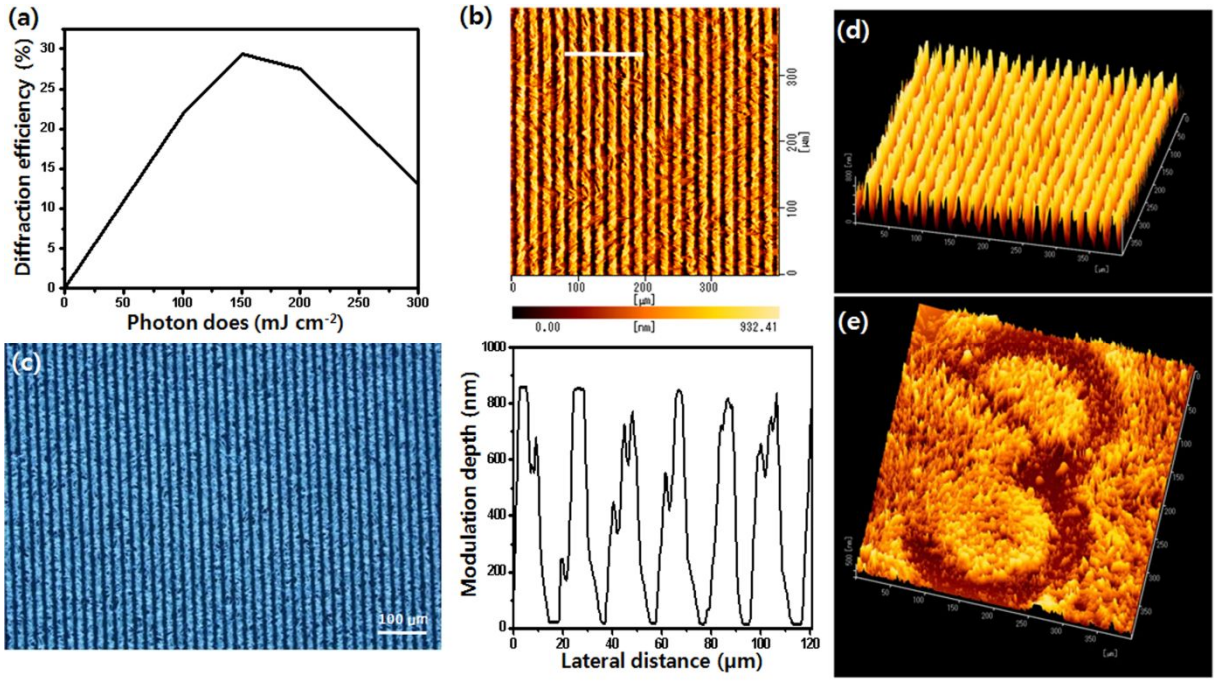

Figure 3.10. Phototriggered surface relief structure on GCS crystalline film: (a) Evaluation of the first order diffraction efficiency as a function of photon does. (b) Topographical AFM image (top) and height profile (bottom) along the white line. (c) Fluorescence optical microscopy image. (d), (e) 3D topological AFM images of surface relief formation according to the photomask.

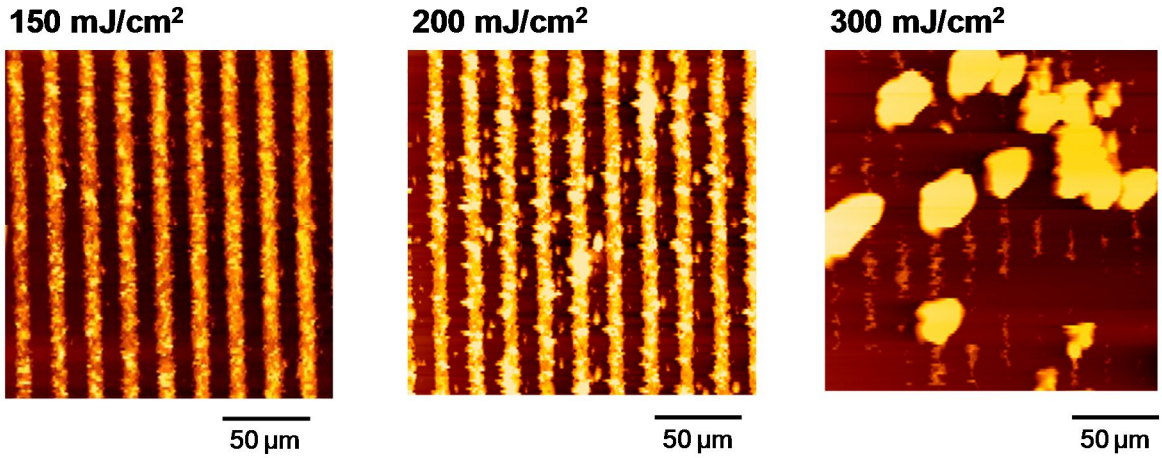

Figure 3.11. AFM images of GCS as a function of photon does.

3.3. Conclusion

We have demonstrated highly fluorescent micropattern based on the phototriggered mass migration in the crystalline film of a cyanostilbene-type fluorescent material. Even at a small photon does (150 mJ cm^{-2}), GCS molecule showed a high diffraction efficiency (~30 %) and a rapid SRG formation (within 150 sec) with a high surface modulation of nearly 200 %. We also suggested the most plausible mechanism of a new type of the phototriggered phase transition, inducing a mass migration and SRG formation. We expect that a novel class of cyanostilbene-containing AIEE molecules will be a highly promising candidate for the fluorescent patterning application due to their intrinsic advantages of an inherent AIEE fluorescence and a phototriggered mass migration. The molecular design using cyanostilbene-type materials for SRG still remains more explorations for the materials development and the understanding of structure-property correlation. Nevertheless, this current achievement of phototriggered mass migration leading to crystallization-induced fluorescence patterning is believed to may open up to new possibilities for the optical information application.

3.4. Experimental

3.4.1. General Information

Materials: All chemicals were purchased commercially, and used without further purification. Synthetic processes are described in the synthesis section.

Characterization: ^{1}H NMR spectra were recorded on a Bruker, Avance-300 (300 Mhz) and Avance-500 (500 Mhz) in CDCl3 solution. Mass spectra were measured using a JEOL, JMS-600W mass spectrometer. Elemental analysis was carried out using a CE instruments, EA1110 elemental analyzer. UV-visible absorption spectra were recorded on a Shimazu, UV-1650 PC spectrometer. Photoluminescence spectra were obtained using a Varian, Cary Eclipse Fluorescence spectrophotometer. The relative fluorescence quantum yield of the GCS solution was measured using 9,10-diphenylanthracence (DPA) in benzene as a standard reference (1×10^{-4} mol L^{-1}, $\Phi_f = 0.83$). The absolute photoluminescence quantum efficiency of the GCS crystalline film was measured using an integrating sphere (Lasphere Co., 600 diameter). DSC measurements were made on a TA Instrument DSC Q 200. The film thickness was estimated by surface profilometry by AFM using a Seiko Nanopics2100 in tapping mode. XRD measurements were achieved with a Rigaku AX-G using a CuKα (0.154 nm) beam. The film sample was placed on a fused silica plate, and the scattered beams were observed on an imaging plate. (The temperature was changed using a Mettler FP-80 stage.) The film state was characterized by GI-XRD measurements. The GI attachment was placed on the FR-E equipment. Light irradiation was performed with a Hg-Xe lamp (UV supercure-203, San-ei Electronic) passing through an appropriate optical filter for 365 nm wavelength selection. Time-resolved fluorescence lifetime experiments were performed by the time-correlated single photon counting (TCSPC) technique with a FluoTime200 spectrometer (Pico- Quant) equipped with a PicoHarp300 TCSPC board (Pico-Quant) and a PMA182 photomultiplier (PicoQuant). The excitation source was a 377 nm picosecond pulsed diode laser

(PicoQuant, LDH375) driven by a PDL800-D driver (Pico-Quant) with fwhm 80 ps. The decay time fitting procedure was carried out with the IRF by using the vFit program (CDP, Russia). The detatiled datas were shown in Figure 3.12.

The time course of phototriggered SRGs was monitored by measuring the changes in the first order diffraction intensity of a helium-neon (He-Ne) laser beam (λ = 633 nm) on the transmission side using a photo-detector with a ADVANTEST TQ8210. The surface topology of the film was observed by AFM.

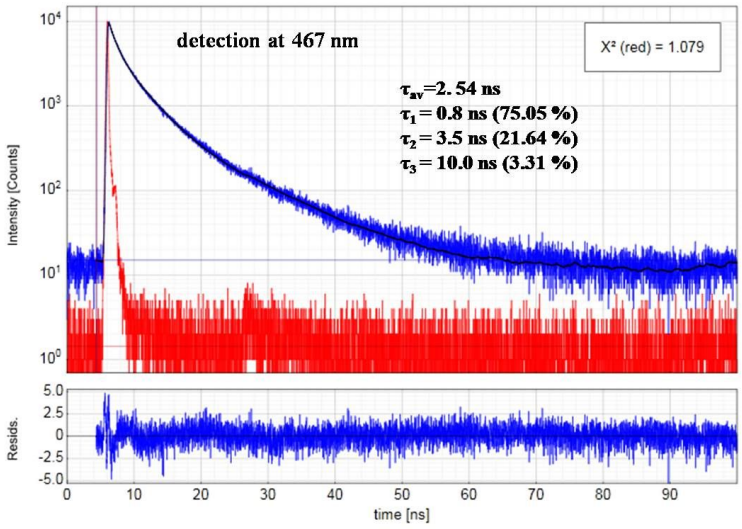

Figure 3.12. Fluorescence decay profiles of the crystal film (black line) and IRF (red line).

3.5. Bibliograrphy

1. a) D. Y. Kim, L. Li, X. L. Jiang, V. Shivshankar, J. Kumar, S. K. Tripathy, *Macromolecules* **1995**, *28*, 8835; b) P. Rochon, E. Batalla, A. Natansohn, *App. Phys. Lett.* **1995**, *66*, 136*;* c) T. Muraoka, K. Kinbara, T. Aida, *Nature* **2006**, *440*, 512*;* d) H. Y. Jiang, S. Kelch, A. Lendlein, *Adv. Mater.* **2006**, *18*, 1471; O. Mermut, C. J. Barrett, *Analyst* **2001**, *126*, 1861.

2. a) J. Isayama, S. Nagano, T. Seki, Macromolecules 2010, 43, 4105; b) P. Che, Y. He, X. Wang, *Macromolecules* **2005**, *38*, 8657; c) R. Ahmed, A. Priimagi, C. F. J. Faul, I. Manners, *Adv. Mater.* **2012**, *24*, 926; d) B. Darracq, F. Chaput, K. Lahlil, Y. Lévy, J.-P. Boilot, *Adv. Mater.* **1998**, *10*, 1133; e) H. Nakano, T. Tanino, Y. Shirota, *App. Phys. Lett.* **2005**, *87*, 061910; f) E. Ishow, B. Lebon, Y. He, X. Wang, L. Bouteiller, L. Galmiche, K. Nakatani, *Chem. Mater.* **2006**, *18,* 1261.

3. T. Seki, Curr. Opin. Solid State Mater. Sci. **2006**, 10, 241.

4. a) L. M. Goldenberg, V. Lisinetskii, Y. Gritsai, J. Stumpe, S. Schrader, *Adv. Mater.* **2012**, *24*, 3339; b) L. H. Liu, K. Nakatani, R. Pansu, J. J. Vachon, P. Tauc, E. Ishow, *Adv. Mater.* **2007**, *19,* 433; c) A. Jacquart, P. Tauc, K. Nakatani, E. Ishow*, J. Mater. Chem.* **2009**, *19*, 8999; d) S. Wu, X. Yu, J. Huang, J. Shen, Q. Yan, X. Wang, W. Wu, Y. Luo, K. Wang, Q. Zhang, *J. Mater. Chem.* **2008**, *18*, 3223.

5. a) B.-K. An, S.-K. Kwon, S.-D. Jung, S. Y. Park, *J. Am. Chem. Soc.* **2002**, *124*, 14410; b) S.-J. Yoon, J. W. Chung, J. Gierschner, K. S. Kim, M.-G. Choi, D. Kim, S. Y. Park, *J. Am. Chem. Soc.* **2010**, *132,* 13675; c) B.-K. An, J. Gierschner, S. Y. Park, *Acc. Chem. Res.* **2011**, *45*, 544; d) S.-J. Yoon, J. H. Kim, K. S. Kim, J. W. Chung, B. Heinrich, F. Mathevet, P. Kim, B. Donnio, A.-J. Attias, D. Kim, S. Y. Park, *Adv. Funct. Mater.* **2012**, *22*, 61.

6. a) A. Gulino, F. Lupo, G. G. Condorelli, M. E. Fragala, M. E. Amato, G. Scarlata, *J. Mater. Chem.* **2008**, *18*, 5011; b) L. Zhu, C. Y. Ang, X. Li, K. T. Nguyen, S. Y. Tan, H. Ågren, Y. Zhao, *Adv. Mater.* **2012**, *24*, 4020.

7. Z. Chen, U. Baumeister, C. Tschierske, F. Würthner, *Chem. Eur. J.* **2007**, *13,* 450.

8. S. Ciorba, G. Galiazzo, U. Mazzucato, A. Spalletti, *J. Phys. Chem. A* **2010**, *114,* 10761.

9. B. Mourey, J. N. Perbet, M. Hareng, S. L. Berre, *Mol. Cryst. Liq. Cryst.* **1982**, *84*, 193.

10. T. Ubukata, S. Fujii, K. Arimatsu, Y. Yokoyama, *J. Mater. Chem.* **2012**, *22*, 14410.

초 록

고형광성 시아노스틸벤 유도체를 기반으로 하는 새로운 광응답성 연성재료: 광물리적 특성 및 액정 거동에 대한 연구

박진욱

재료공학부

The Graduate School

Seoul National University

광반응 물질들은 광학장치, 그리고 광액추에이터 등의 다양한 범위에 응용성 때문에 유망한 연구주제 이다. 특히, 이러한 응용을 구현하기 위해서 빠르고 가역적인 광에 의해 야기되는 기하이성질체 특성을 보여주는 아조벤젠, 그리고 스틸벤 연성재료들이 알려져 있다. 이러한 특별한 특성들에도 불구하고, 위 재료들은 고상에서 형광 특성이 낮거나 혹은 없는 특성을 보여준다. 이러한 문제를 해결 하기 위해, 형광성 염색재료들을 아조벤젠 또는 스틸벤 구조에 일차적인, 이차적인 결합 상호작용, 또는 호스트-게스트 (host-guest) 방식을 통해서 붙여준다. 그럼에도 불구하고, 현재까지, 오직 성공적인 현상을 보여준 것은 거의 없다.

현재까지, 우리 그룹에서는 용액상태에서는 형광이 없는 상태이지만 고상이 되면서 자가조립에 의한 초분자체를 형성하면서 강한 형광이 발현되는 AIEE라는 특성을 보여주는 α-시아노-치환체인 스틸벤 유도체들에 대한 연구들을 보고해왔다. 게다가, 이러한 물질들은 아조벤젠, 스틸벤 물질처럼 광조사에 따라 트랜스(trans)-시스(cis)의 기하이성질체를 형성하는 특성을 보여주게 된다. 그러나, 이러한 물질들을 이용하여 기하이성질체 거동과 형광 특성사이에 대한 보고 내용은 아직 없다.

따라서, 우리는 시아노스틸벤 파생물들을 기반으로 한 액정 혹은 연성결정상에서의 광유도 기하이성질체 특성을 이용한 형광성 패터닝 기술 구현을 보고하고자 한다. 고상에서의 광 유도 기하이성질체 반응이 효율적으로 나타나도록 하기 위하여 자유부피(free volume)의 변동을 야기하는 액정시스템이 도입되었다. 물질들은 rigid하며 광 기하이성질체 특성 및 AIEE 거동을 보여주는 시아노스틸벤/다이시아노스티릴벤젠(DCS) 구조와 유동성을 가지는 alkoxy 치환기를 다양한 길이 별로 구성되었다. 이 점에서, 액정상과 고상에서의 광학특성에 대한 완전한 이해를 하기 위해서, 우리는 다음과 같은 내용을 연구하고자 한다: i) CN 그룹의 역할, ii) 알킬 길이에 역할, 그리고 (iii) 시아노스틸벤과 다이시아노스틸벤 구조 사이에 기하이성질체의 거동 차이에 대한 이해. 광 기하이성질체 특성은 UV-visible 흡수 스펙트라에 변화를 통해서 확인할 수 있었고 트랜스(trans)에서 시스(cis)형태로의 전환 비율을 ^{1}H NMR 데이터 분석을 통해 확인할 수 있었다. 이러한 특성을 기반으로, 형광 패턴 이미지를 구현하였다.

게다가, 우리는 상온에서 columnar hexagonal 액정 상을 나타내는 새로운 시아노스틸벤 구조를 기반으로하는 물질, GCS라는 물질을 합성하였다. GCS의 얇은

필름은 스핀-코팅 방법을 통하여 준비 되었다. 처음에, 만들어진 필름은 높은 투명도를 가지는 무정형상태로 보여진다. 그러나, 시간이 지남에 따라 부분적인 결정화가 나타나게 된다. 상온 근처 (25~30 ℃)에서 하루 정도 지나게 되면, GCS의 파우더 결정 상태와 같은 결정상을 가지는 균일한 결정상태의 필름이 된다. 결정상태에서, GCS는 강한 파란색의 형광을 나타낸다. 흥미롭게도, 이 결정 상태는 연성 특성을 보여준다. 이러한 특성을 이해하기 위해, 우리는 GI-XRD 측정을 진행하였다. 연성 상태에서, GCS는 광 기하이성질체 과정을 통한 상변화를 보여주게 된다. 따라서, 우리는 연성 결정 물질을 이용하여 광 기하이성질체 특성으로 나타나는 상변화를 동반한 집단 이동(mass migration)이라는 독특한 현상을 이용하여 고 형광성 마이크로 패턴들을 나타내는데 성공하였다. 본 연구에서, 우리는 결정에서 액정상으로의 상변화를 동반한 집단 이동(mass migration)이라는 새로운 메커니즘을 처음으로 제시한다.

주요어: 액정, 광유도 기하이성질체, 형광 패터닝, 집단 이동, 표면 요철 격자

학 번: 2011-20645

List of Presentation

1. Jinwook Park, Seong Jun Yoon, Soo Young Park, "Highly Lumunescent Novel Soft Material Based on Cyanostilbene Molecule: Mesomorphic Organization at Room Temperature and Surface Relief Grating with Enhanced Flourescence Emission ", 2012 춘계학술대회 한국고분자학회, 대전컨벤션센터, 2012-04-12

2. Jinwook Park, Soo Young Park, "Phototriggered Mass Migration Leading to Aggregation Induced Fluorescence Patterning in Discotic Cyanostilbene Thin Films", 2012 대한화확회 제110회 추계학술발표회, 부산(벡스코), 2012-10-17